

ComBAT Harmonization for diffusion MRI: Challenges and Best Practices

Pierre-Marc Jodoin^{1,2,*}, Manon Edde^{1,3}, Gabriel Girard¹, Félix Dumais¹,
Guillaume Theaud², Matthieu Dumont², Jean-Christophe Houde²,
Yoan David¹, Maxime Descoteaux^{1,2}, Alzheimer's Disease Neuroimaging Initiative⁴

¹Université de Sherbrooke, 2500 Boul. de l'Université, J1K 2R1 Sherbrooke, Qc, Canada

²Imeka Solutions inc, 195 Belvédère nord, J1H 4A7, Sherbrooke, Qc, Canada

³StoP-AD Centre, Douglas Mental Health University Institute, McGill University, Montréal, H4H 1R3, Quebec, Canada

⁴Data used in preparation of this article were obtained from the ADNI database (adni.loni.usc.edu).

Abstract

Over the years, ComBAT has become the standard method for harmonizing MRI-derived measurements, with its ability to compensate for site-related additive and multiplicative biases while preserving biological variability. However, ComBAT relies on a set of assumptions that, when violated, can result in flawed harmonization. In this paper, we thoroughly review ComBAT's mathematical foundation, outlining these assumptions, and exploring their implications for the demographic composition necessary for optimal results.

Through a series of experiments involving a slightly modified version of ComBAT called Pairwise-ComBAT tailored for normative modeling applications, we assess the impact of various population characteristics, including population size, age distribution, the absence of certain covariates, and the magnitude of additive and multiplicative factors. Based on these experiments, we present five essential recommendations that should be carefully considered to enhance consistency and supporting reproducibility, two essential factors for open science, collaborative research, and real-life clinical deployment.

Introduction

In neuroimaging, leveraging multi-site data to analyze general trends and variability within diverse populations is increasingly common [1, 2, 3, 4, 5]. However, variations in imaging protocols across sites introduce systematic biases, posing significant challenges to multi-site and longitudinal studies [6, 7, 8, 9, 10, 11, 12, 13]. To address these biases, various harmonization techniques have been developed [13, 14, 15, 16, 7, 17, 18, 19]. These methods either pre-harmonize diffusion-weighted images via neural networks or other techniques like LinearRISH [9, 20, 21] or post-harmonize MRI-derived measurements, such as through ComBAT [18, 19, 22].

ComBAT is one of the most effective methods (8,000+ citations as of March 2025 according to PubMed) for harmonizing MRI-derived measurements due to its ease of application and ability to adjust for site-related additive and multiplicative biases while preserving biological variability [23, 22, 24, 25]. Its success has led to the development of various ComBAT-like methods, such as Longitudinal ComBAT [26], CovBat [14], Auto-ComBAT [27], GMM-ComBAT [16], M-ComBAT [28], and ComBAT-GAM [29], Cluster-ComBAT [30], each offering specific improvements. Despite these advances, the orig-

inal ComBAT remains a widely used solution in both research and clinical research applications [23, 22, 31].

ComBAT relies on several key assumptions, which researchers have highlighted in previous studies. Failing to meet these assumptions can significantly impact its effectiveness. The primary assumptions include:

1. The covariate effects (i.e. sex, age, handedness, etc.) on the data must be consistent across all harmonization sites (more details in § Theory).
2. The population distributions must be uniform across sites, with no substantial imbalances in key covariates (i.e., sample, age, sex, medical condition) [11, 32, 33].
3. Age distributions must overlap substantially across sites and span a wide age range [26, 29].
4. Harmonization studies are limited to a manageable number of sites, and data can be harmonized in a single step once the data acquisition is complete.

Unfortunately, these assumptions are often overlooked in practice. Notably, no study has systematically evaluated their impact on ComBAT's performance under controlled conditions or provided clear, quantifiable guidelines in diffusion MRI.

In this paper, we thoroughly review ComBAT's mathematical foundation, clarifying its assumptions

*Corresponding author: jane@smith.com

and the demographic conditions necessary for optimal performance. We also argue that aligning each site with a common reference dataset, with a method called *Pairwise-ComBAT*, mitigates some of ComBAT’s limitations. Doing so enhances consistency and supporting reproducibility, two essential factors for open science, collaborative research, and real-life clinical deployment.

Throughout our experiments, we use the Cambridge Centre for Ageing Neuroscience dataset (CamCAN) [34, 35], as a reference dataset and evaluate the impact of the magnitude additive and multiplicative bias, and various demographic characteristics including sample size, age distribution, missing covariates and pathological population presence. In some cases, we replicate our results with other public databases, such as the Alzheimer’s Disease Neuroimaging Initiative (ADNI) [36] dataset or the Mind Research Network (MRN, site A) dataset [37]. To assess the harmonization quality, we also proposed a goodness-of-fit measure mathematically derived from *Pairwise-ComBAT*.

Following these experiments, we present five essential recommendations to use ComBAT. This paper aims to highlight both the limitations and opportunities that ComBAT presents for multi-site data harmonization.

Theory

In this section, we present the theory behind ComBAT. We outline the parameters of ComBAT, how they are estimated, and how they are used to harmonizing data. To ensure a good understanding of the method, the reader shall refer to Figure 1 for the key harmonization steps. Note that although this figure is tailored to *Pairwise-ComBAT* (c.f. §*Pairwise-ComBAT*), it can be used to demystify ComBAT’s formalism.

Let $\mathcal{Y} = \{Y_1, \dots, Y_I\}$ be a set of I physical MRI sites and $Y_i = \{Y_{i1}, \dots, Y_{ij_i}\}$ the J_i dMRI derived metric images from the site i . For example, Y_i may contain a set of FA maps obtained from the same MRI system at site i . Note that J_i is site dependent, as the number of data is usually different from one site to another. Each map Y_{ij} can be represented as $Y_{ij} = [y_{ij1}, \dots, y_{ijV}]$, where V is the number of voxels (or regions) in the common space and $y_{ijv} \in \mathbb{R}$.

To compensate for site-specific biases, ComBAT uses a linear model for the data formation of each voxel (or region) v as follows:

$$y_{ijv} = \alpha_v + \mathbf{x}_{ij}^T \boldsymbol{\beta}_v + \gamma_{iv} + \delta_{iv} \varepsilon_{ijv}, \quad (1)$$

where α_v is the model intercept of the overall population across all sites, \mathbf{x}_{ij} is a vector of covariates

(i.e. age and sex), $\boldsymbol{\beta}_v$ is a regression vector, γ_{iv} is the additive site effect, δ_{iv} is the multiplicative site effect, and ε_{ijv} is some random independent Gaussian noise with $\varepsilon_{ijv} \sim \mathcal{N}(0, \sigma_v^2)$. This model is illustrated for two sites in Figure 1(b) where the black line corresponds to the overall population trend represented by $\boldsymbol{\beta}_v$ in the previous equation. It is crucial to recognize that ComBAT assumes the regression vector $\boldsymbol{\beta}_v$ (i.e. the slope of the population) is constant for all sites which, as will be demonstrated, is often incorrect and results in flawed harmonization functions. Thus, the harmonization process of two parallel black and red populations illustrated in figure 1(b) is an idealized version of the algorithm.

The primary goal of ComBAT is to eliminate the site-specific additive and multiplicative biases (respectively γ_{iv} and δ_{iv}) ensuring that the harmonized population profile conforms to the black dotted model depicted in Figure 1(j):

$$y_{ijv}^{\text{ComBAT}} = \alpha_v + \mathbf{x}_{ij}^T \boldsymbol{\beta}_v + \varepsilon_{ijv}. \quad (2)$$

Since each parameter of the model $\alpha_v, \boldsymbol{\beta}_v, \gamma_{iv}, \sigma_v$ and δ_{iv} are a priori unknown, they must be empirically estimated from the data. One simplistic approach to estimating these parameters is through the L/S-ComBAT (Location and Scale) method [18]. Although this approach is straightforward, it has its share of limitations which are typically addressed with the Bayesian formulation of ComBAT which is simply called *ComBAT* in Fortin et al. (2017) [19].

ComBAT starts by computing the regression vector $\boldsymbol{\beta}_v$ and the intercept α_v with an ordinary least-square approach

$$[\hat{\alpha}_v, \hat{\boldsymbol{\beta}}_v] = (X^T X)^{-1} X^T Y_v, \quad (3)$$

where X is the matrix of covariate vectors from every participant across all sites, and Y_v is a vector containing the metric in location v for every participant in all sites.

ComBAT standardizes all data in relation to $\hat{\alpha}_v$ and $\hat{\sigma}_v$ as depicted in Figure 1(d) and represented mathematically as

$$z_{ijv} = \frac{y_{ijv} - \hat{\alpha}_v - \mathbf{x}_{ij}^T \hat{\boldsymbol{\beta}}_v}{\hat{\sigma}_v}, \quad (4)$$

where $\hat{\sigma}_v$ is given by

$$\hat{\sigma}_v^2 = \frac{1}{J_I} \sum_{ij} (y_{ijv} - \hat{\alpha}_v - \mathbf{x}_{ij}^T \hat{\boldsymbol{\beta}}_v - \hat{\gamma}_{iv})^2, \quad (5)$$

where J_I is the total number of data across every site. Then, ComBAT estimates γ_{iv}^* and δ_{iv}^{2*} by maximizing their posterior distribution instead of their

Pairwise-ComBat Harmonization Steps – Simulated Data

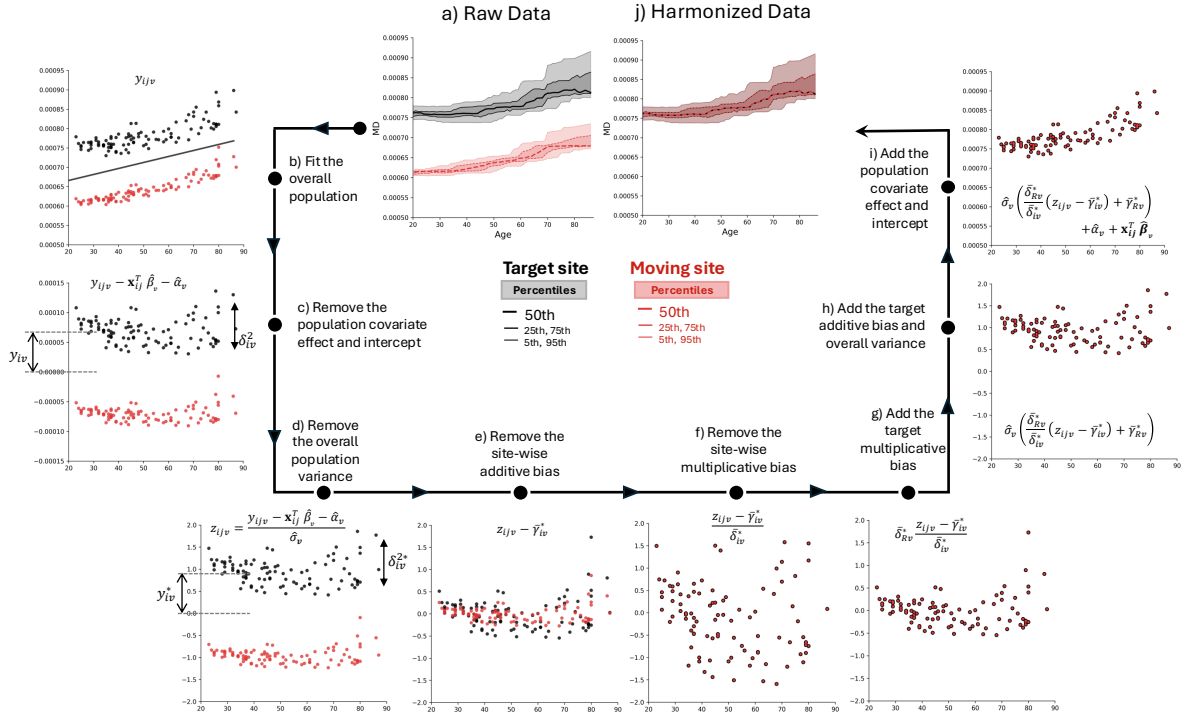


Figure 1: Illustration of the seven steps of a typical Pairwise-ComBAT harmonization of two sites underlying the effect of each variable of Eq.(17). From the raw data in a) to the harmonized data in i). The gray curves in b) illustrate the overall trend of the population from site 1 and site 2, whereas the scatter plots show the values of the J subjects of each site.

likelihood distribution as in L/S ComBAT[18]¹. Following Bayes' theorem, the posteriors γ_{iv}^* and δ_{iv}^{2*} can be written as

$$\pi(\gamma_{iv}^* | \mathbf{z}_{iv}, \delta_{iv}^{2*}) \propto L(\mathbf{z}_{iv} | \gamma_{iv}^*, \delta_{iv}^{2*}) P(\gamma_{iv}^*), \quad (6)$$

$$\pi(\delta_{iv}^{2*} | \mathbf{z}_{iv}, \gamma_{iv}^*) \propto L(\mathbf{z}_{iv} | \gamma_{iv}^*, \delta_{iv}^{2*}) P(\delta_{iv}^{2*}), \quad (7)$$

where

$$L(\mathbf{z}_{iv} | \gamma_{iv}^*, \delta_{iv}^{2*}) = \mathcal{N}(\gamma_{iv}^*, \delta_{iv}^{2*}) \text{ (likelihood - Gaussian)}$$

$$P(\gamma_{iv}^*) = \mathcal{N}(\mu_i, \tau_i^2) \text{ (prior - Gaussian)}$$

$$P(\delta_{iv}^{2*}) = \mathcal{IG}(\lambda_i, \theta_i) \text{ (prior - Inverse Gamma)}.$$

The hyperparameters of the prior distributions μ_i , τ_i^2 , λ_i , and θ_i are estimated following the moment of these distributions. As such, μ_i and τ_i^2 are the empirical mean and variance across every location v of site i ,

$$\bar{\mu}_i = \frac{1}{V} \sum_v \hat{\gamma}_{iv}^*, \quad \bar{\tau}_i^2 = \frac{1}{V-1} \sum_v (\hat{\gamma}_{iv}^* - \bar{\mu}_i)^2, \quad (8)$$

where $\hat{\gamma}_{iv}^* = \frac{1}{J_i} \sum_j z_{ijv}$ is the location-wise and site-wise average of the **standardized** data illustrated in figure 1(d) and (e).

¹ ComBAT notation can be confusing. While γ_{iv} and δ_{iv}^2 are the bias and variance of the rectified population (fig. 1(c)), γ_{iv}^* and δ_{iv}^{2*} are bias and variance of the standardized populations of fig. 1(d)

The estimation of λ_i and θ_i , one first need to compute the voxel-wise and site-wise standardized variance $\delta_{iv}^{2*} = \frac{1}{J_i-1} \sum_j (z_{ijv} - \hat{\gamma}_{iv}^*)^2$. The empirical mean and variance of δ_{iv}^{2*} across all location v is computed as $\bar{G}_i = \frac{1}{V} \sum_v \delta_{iv}^{2*}$ and $\bar{S}_i^2 = \frac{1}{V-1} \sum_v (\delta_{iv}^{2*} - \bar{G}_i)^2$. Then, by having \bar{G}_i and \bar{S}_i^2 equal to the first and second theoretical moment of the inverse gamma distribution, we get

$$\bar{G}_i = \frac{\theta_i}{\lambda_i - 1}, \quad \bar{S}_i^2 = \frac{\theta_i^2}{(\lambda_i - 1)^2 (\lambda_i - 2)} \quad (9)$$

that can be rearranged as follows to get the estimate of the two hyperparameters

$$\bar{\lambda}_i = \frac{\bar{G}_i^2 + 2\bar{S}_i^2}{\bar{S}_i^2}, \quad \bar{\theta}_i = \frac{\bar{G}_i^3 + \bar{G}_i \bar{S}_i^2}{\bar{S}_i^2}. \quad (10)$$

Now that the hyperparameters of the likelihood and prior distributions have been estimated, by developing eq.(6) and (7) and combining to it eq. (8) and (10) to it, we get that the mathematical expectation of the posterior distributions lead to the following estimate of γ_{iv}^* and δ_{iv}^{2*}

$$\hat{\gamma}_{iv}^* = \hat{\mathbb{E}}(\gamma_{iv}^* | \mathbf{z}_{iv}, \delta_{iv}^{2*}) = \frac{J_i \bar{\tau}_i^2 \hat{\gamma}_{iv}^* + \delta_{iv}^{2*} \bar{\mu}_i}{J_i \bar{\tau}_i^2 + \delta_{iv}^{2*}} \quad (11)$$

$$\hat{\delta}_{iv}^{2*} = \hat{\mathbb{E}}(\delta_{iv}^{2*} | \mathbf{z}_{iv}, \gamma_{iv}^*) = \frac{\bar{\theta}_i + \frac{1}{2} \sum_j (z_{ijv} - \hat{\gamma}_{iv}^*)^2}{\frac{J_i}{2} + \bar{\lambda}_i - 1}. \quad (12)$$

Since equations (11) and (12) are inter-dependent, $\tilde{\gamma}_{iv}^*$ and $\hat{\delta}_{iv}^{2*}$ are estimated through an iterative process by starting with a reasonable value for $\hat{\delta}_{iv}^{2*}$ (i.e., $\hat{\delta}_{iv}^{2*}$), then by calculating $\tilde{\gamma}_{iv}^*$, and then by re-estimating $\hat{\delta}_{iv}^{2*}$ with the new value of $\tilde{\gamma}_{iv}^*$ and so on. This process is repeated until converges.

Once all parameters of eq.(1) have been empirically estimated, the data can be harmonized as follows :

$$y_{ijv}^{ComBAT} = \frac{\hat{\sigma}_v}{\hat{\delta}_{iv}^{2*}} (z_{ijv} - \tilde{\gamma}_{iv}^*) + \hat{\alpha}_v + \mathbf{x}_{ij}^T \hat{\beta}_v, \quad (13)$$

as illustrated in Figure 1(f) to (i).

Mathematical limitations of ComBAT

The slope β_v As outlined through the previous equations, ComBAT assumes that the slope β_v is the same for all sites' region v . This assumption is problematic when the canonical data formation model of Eq.(2) is affected by a multiplicative factor S_i and an additive factor A_i as follows:

$$\begin{aligned} y_{ijv} &= y_{ijv}^{ComBAT} * S_i + A_i \\ &= \alpha_v S_i + A_i + \mathbf{x}_{ij}^T \beta_v S_i + \epsilon_{ijv} S_i \\ &= \alpha_v + \gamma_{iv} + \mathbf{x}_{ij}^T \beta_v S_i + \delta_{iv} \epsilon_{ijv}, \end{aligned} \quad (14)$$

where $\gamma_{iv} = \alpha_v(S_i - 1) + A_i$ and $\delta_{iv} = S_i$. While Eq. (14) is similar to Eq. (1), it nonetheless contains a multiplicative term S_i on the slope which is not taken care of by ComBAT. As will be shown later, this results into misalignment populations when the uniform slope assumption is violated.

The variance δ_{iv}^{2*} When calculating the variance $\hat{\delta}_{iv}^{2*}$, two key considerations ought to be taken into account. First, the posterior estimator of Eq. (12) can be viewed as a nonlinear weighted average of the empirical and prior variances with respect to the J_i (i.e. the number of data at site i). To illustrate that, when $J_i \rightarrow 0$, Eq. (12) becomes $\hat{\delta}_{iv}^{2*} \rightarrow \frac{\hat{\theta}_i}{\lambda_i - 1}$, which, in combination with Eq. (10), yields to $\hat{\delta}_{iv}^{2*} \approx \hat{G}_i$, representing the prior variance. Conversely, as $J_i \rightarrow \infty$, Eq. (12) simplifies to $\hat{\delta}_{iv}^{2*} \rightarrow \frac{1}{J_i} \sum_j (z_{ijk} - \gamma_{iv})^2$, the formula for empirical variance. However, as we will demonstrate empirically, the weight assigned to the prior term remains disproportionately high as J_i increases. As a consequence, a poor a priori variance \hat{G}_i will affect $\hat{\delta}_{iv}^{2*}$ even on large populations of more than ~ 100 subjects.

The second consideration that one must keep in mind is the fact that the variance $\hat{\delta}_{iv}^{2*}$ depends on z_{ijv} . Since z_{ijv} is itself influenced by $\mathbf{x}_{ij}^T \beta_v$ (c.f. Eq. (4)), whenever the slope assumption is violated, the term $(z_{ijv} - \tilde{\gamma}_{iv}^*)^2$ becomes biased, leading to an inaccurate estimation.

Method

For the need of a reference site

ComBAT harmonizes multisite data by projecting each data point onto an "average" site, defined by an intercept $\hat{\alpha}_v$, a slope $\hat{\beta}_v$, and a variance $\hat{\sigma}_v^2$ (Eq. (13)), illustrated by the black line in Fig. 1(b). This approach is ideal for structured studies or clinical trials, in which participants undergo specific interventions according to a predefined protocol, with data collected at multiple sites under controlled conditions. Additionally, such studies are usually time-bound, culminating with a fixed set of sites and participants that are harmonized collectively at the end of the study.

However, many applications do not meet these constraints. We argue that aligning each site to a common reference dataset, ideally one that is well populated across all covariates, offers a more versatile and robust solution. There are three main reasons for adopting this approach.

i) Reproducibility and open science Harmonizing data to a reference dataset offers multiple advantages for the scientific community. First, it allows for the creation of openly accessible and readily usable datasets, as it enhances the comparability of data collected from diverse sources. This eliminates the need for future re-harmonization and simplifies data sharing processes. By aligning with a common reference site, researchers can also establish reproducible standards for critical imaging metrics, such as those in diffusion MRI, which play a key role in characterizing disease. This reproducibility is essential to open science, fostering transparent and collaborative research across institutions. Additionally, harmonization to a reference site facilitates longitudinal studies, where data collection spans extended periods. When new data are harmonized to the same reference, researchers can confidently track disease progression or treatment outcomes without concerns about changing the harmonization parameters. This stability supports the robustness of findings over time and reduces the computational resources needed for repeated harmonization.

ii) Normative modeling Normative modeling quantifies individual variability by assessing how much a subject deviates from a representative population. Typically, a normative model is built by pooling data across sites. Since ComBAT's parameters (α_v , β_v , and σ_v) are computed from all sites' data, adding new data to the pool shifts the average reference site, creating a "moving target" issue. Although Kia et al. propose a hierarchical Bayesian regression (HBR) ap-

proach to mitigate this effect [38], this approach cannot be used to harmonize data. Also, we suggest that harmonizing each site pairwise to a stable reference dataset is a much simpler approach for building a normative reference model than the iterative and cyclic approach that HBR is built upon.

iii) Routine clinical practice Clinical practice entails a continuous flow of data from numerous, and potentially expanding, sources over an indefinite period. For software providers, this results in the need to accommodate unpredictable growth in data sources. This variability challenges the traditional ComBAT harmonization method. By independently harmonizing each site to a common reference, new sites can be seamlessly integrated as they come online, avoiding the common ComBAT issue where the harmonization of a new site disrupts the parameters already established for previously harmonized sites. Furthermore, once harmonization parameters are set for a site, they can be applied to incoming data from that site, thus reducing the need for repeated harmonization efforts.

In our experiments, we examine how limited data at either the target or reference site, restricted age ranges, and undocumented diseases affect ComBAT's performance. Unlike previous studies that focus solely on training error, we treat harmonization as a machine learning problem with distinct training and testing sets. This approach enables us to evaluate ComBAT's generalization to new, unseen data, providing a more comprehensive assessment of its effectiveness.

Pairwise-ComBAT

The goal of *Pairwise-ComBAT* is to harmonize each moving site, denoted as M , independently onto a reference site, R . The reference site acts as a standardized baseline, containing diverse data representative of healthy individuals.

To achieve this, data from site M is harmonized using the parameters of site R , specifically the multiplicative (δ_{Rv}^*) and additive (γ_{Rv}^*) batch effects. This results in a modified version of Eq. (13):

$$y_{Mjv}^{ComBAT} = \hat{\sigma}_v \left(\frac{\delta_{Rv}^*}{\delta_{Mv}^*} (z_{Mjv} - \tilde{\gamma}_{Mv}^*) + \tilde{\gamma}_{Rv}^* \right) + \hat{\alpha}_v + \mathbf{x}_{Rj}^T \hat{\beta}_v. \quad (15)$$

For a more intuitive understanding of Pairwise-ComBAT, the reader may refer to Figure 1, particularly panels (f) to (i), which illustrate the effect of each parameter.

While Pairwise-ComBAT is conceptually similar to Da-Ano et al's M-ComBAT [28], our harmonization equation (Eq. (15)) differs from their's (Eq. (4) in

paper [28]). Furthermore, in all our experiments, we assume the reference site is well-populated, an assumption not made by Da-ano et al.

The reader shall note that Pairwise-ComBAT is only a reconfiguration of the original ComBAT method, thus producing an equivalent harmonization outcome with the same strengths and weaknesses as the original ComBAT [19].

Goodness of fit

To gauge the performances of ComBAT, we propose a goodness-of-fit metric that measures how well two populations overlap. By assuming that the moving (M) and reference (R) populations are well harmonized, our method rectifies both populations using the reference parameter intercept $\tilde{\gamma}_{Rv}^*$, i.e. :

$$\begin{aligned} z_{Rjv} &= y_{Rjv} - \hat{\alpha}_v - \tilde{\gamma}_{Rv}^* - \mathbf{x}_{Rj}^T \beta_v & \forall y_{Rjv} \in T_{Tv} \\ z_{Mjv} &= y_{Mjv}^{ComBAT} - \hat{\alpha}_v - \tilde{\gamma}_{Rv}^* - \mathbf{x}_{Mj}^T \beta_v & \forall y_{Mjv} \in Y_{Mv} \end{aligned}$$

By removing the effect of the covariates and the biases, this rectification allows assuming that z_{ijv} is independent from \mathbf{x}_{ij} and that $P(z_{Rjv} | \mathbf{x}_{Rj}) = P(z_{Rjv})$ and $P(z_{Mjv} | \mathbf{x}_{Mj}) = P(z_{Mjv})$ which is Gaussian as mentioned after eq. (7). The distance between univariate distribution is computed using the Bhattacharyya distance (BD) which, in the case of two Gaussian distributions, results into the following closed-form solution

$$d(P(z_{Rjv}) | P(z_{Mjv})) = \frac{1}{4} \frac{(\mu_{Tv} - \mu_{Mv})^2}{(\sigma_{Rv}^2 + \sigma_{Mv}^2)} + \frac{1}{2} \ln \left(\frac{\sigma_{Tv}^2 + \sigma_{Mv}^2}{2\sigma_{Tv} + \sigma_{Mv}} \right)$$

where $\mu_{Rv} = \text{mean}_j(z_{Rjv})$, $\mu_{Mv} = \text{mean}_j(z_{Mjv})$, $\sigma_{Rv}^2 = \text{var}_j(z_{Rjv})$, and $\sigma_{Mv}^2 = \text{var}_j(z_{Mjv})$.

An illustration of the BD computed before and after harmonization is provided in Figure 2.

Dataset studied

Reference site

The public CamCAN Stage 2 dataset [34, 35] is a large-scale, multi-modal study investigating cognitive aging across the adult lifespan (ages 18 – 87) using MRI, MEG, and cognitive data. With roughly 700 participants, the sample is well-balanced, thanks to a uniform age and sex distribution and recruitment from a larger population-based cohort of 2681 individuals [35]. Approval for the study was granted by the Research Ethics Committee of Cambridgeshire 2 (reference: 10/H0308/50 [34]), and participants gave written, informed consent prior to involvement. A total of 441 healthy participants (224 males, 217 females) were selected for this study.

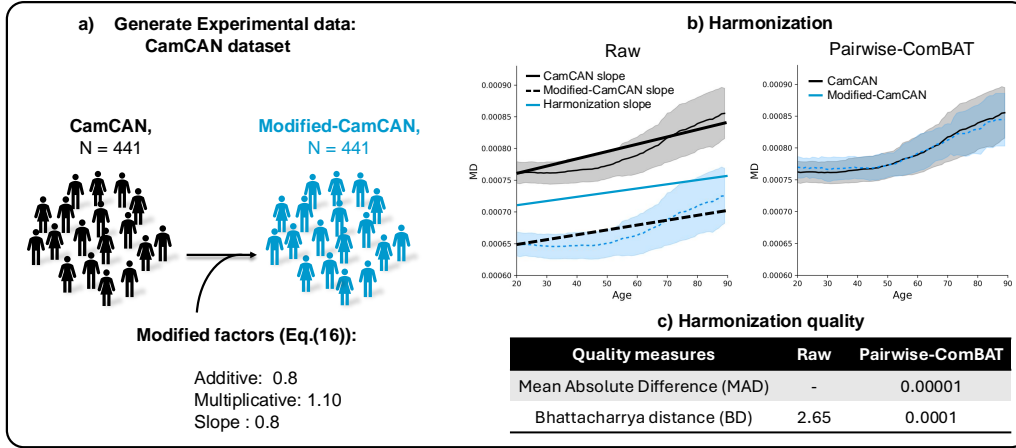


Figure 2: Pairwise-ComBAT harmonization of the mean diffusivity (MD) in the modified CamCAN dataset against the unbiased CamCAN ($N=441$). (a) The parameters A (additive), M (multiplicative), S (slope) used to generate the modified CamCAN version (c.f. Eq.(16)). (b) (left) raw data with the slopes for CamCAN (solid black line), modified CamCAN (dashed black line), and the slope estimated by Pairwise-ComBAT (solid blue line). (right) The Pairwise-ComBAT harmonization. (c) Distances between the raw and harmonized populations.

DWI data were acquired on a 3T Siemens TIM Trio Scanner (32-channel head coil) using a twice refocused spin echo (TRSE) echo-planar imaging sequence to reduce eddy-current artifacts. The acquisition included two b-values of 1000 and 2000 s/mm² along 30 directions and three non-diffusion-weighted images ($b=0$). Additional parameters were: 66 axial slices, voxel size = 2 mm x 2 mm x 2 mm, repetition time (TR) = 9100 ms, echo time (TE) = 104 ms, and an acceleration factor of 2 using GRAPPA [35].

Moving sites

Modified-CamCAN This dataset contains the same data as the CamCAN dataset but with different additive and multiplicative biases following this equation:

$$y_{ijv} = \alpha_v + \gamma_{iv}A + \mathbf{x}_{ij}^T \beta_v S + \delta_{iv} \epsilon_{ijv} M \quad (16)$$

where A is used to translate the population, S to change the slope of the population wrt their associated covariates and M to change the variance of the population.

An example of CamCAN and modified CamCAN (both with 441 subjects) with $A = 0.8$, $S = 0.8$ and $M = 1.1$ is illustrated in Figure 2(a). Figure 2(b) shows the two population distributions before (left) and after (right) the Pairwise-ComBAT harmonization. In Figure 2(c), we have the BD metrics and mean absolute difference (MAD) between the moving and the reference site data points before and after harmonization. This figure echoes with most experiments reported in § Results.

ADNI The ADNI data were obtained from the Alzheimer’s Disease Neuroimaging Initiative (ADNI)

database². The ADNI was launched in 2003 as a public-private partnership, led by Principal Investigator Michael W. Weiner, MD. The primary goal of ADNI has been to test whether serial magnetic resonance imaging (MRI), positron emission tomography (PET), other biological markers, and clinical and neuropsychological assessment can be combined to measure the progression of mild cognitive impairment (MCI) and early Alzheimer’s disease (AD).

We selected the 152 subjects (100 Healthy Control (HC), 28 Mild Cognitive Impairment (MCI), 24 Alzheimer’s Disease (AD)) from site 127-GE site of the ADNI-3 cohort [36]. ADNI-127-GE includes 83 males and 69 females, with age mean/std of 73.4 ± 7.4 (Min: 61, Max: 90), 142 subjects were left-handed and 11 right-handed.

The diffusion weighted MRI (DWI) data were acquired on a 3T General Electric (GE) Healthcare using a spin echo imaging sequence. Acquisition includes 6 non-diffusion-weighted images ($b=0$) and 48 directions with b-value of 1,000 s/mm². Additional parameters are: TE =56 ms, TR =7800 ms, voxel size = 2 mm x 2 mm x 2 mm and approximate scan time =7 min 30 s.

NIMH We used the 157 subjects from the National Institute of Mental Health (NIMH) Intramural Healthy Volunteer Dataset [39]. The MRI protocol used was initially based on the ADNI-3 basic protocol and was modified for DWI acquisition to include the slice-select gradient reversal method and reversed blip scans; and turned off reconstruction interpolation. The 3D-T1 weighted acquisition from ADNI-3 was replaced by the 3D-T1 acquisition from

² adni.loni.usc.edu

the ABCD protocol. All participants provided electronic informed consent for online pre-screening, and written informed consent for all other procedures.

Processing

The same tractoflow pipeline [40] was used to process the datasets. b-values below $b = 1200 \text{ ms}/\text{m}^2$ were used to compute DTI-derivatives scalar maps and b-values above $b = 700 \text{ ms}/\text{m}^2$ were used to compute fiber orientation distribution function (fODF) metrics scalar maps. The fODF was generated using a spherical harmonics order of 8 and the same fiber response function [41] for all the subjects $(15, 4, 4) \times 10^4 \text{ ms}/\text{m}^2$. Next, all metrics were registered to the Montreal Neurological Institute (MNI) space. The IIT Human Brain Atlas (IIT-FA-skeleton, v.5.0, [42]) was finally used to extract the averaged value for each major white matter fiber bundle of interest ($N=25$).

For simplicity and ease of reading, the results section presents only one white matter bundle, the arcuate fascicles left (AF left), and a single diffusion metric derived from the Diffusion Tensor Imaging (DTI) model, the mean diffusivity (MD).

Harmonization of the experimental data

As mentioned before, we consider ComBAT as a machine learning algorithm. As such, every dataset was divided into 2 subsets: a training subset used to estimate the harmonization parameters $\hat{\sigma}_v, \hat{\delta}_{iv}^*, \hat{\gamma}_{iv}^*, \hat{\alpha}_v$ and $\hat{\beta}_v$, and a test subset to gauge the generalization capabilities of ComBAT. In all cases, CamCAN was used as the reference site towards which each dataset is harmonized to. In the case of modified-CamCAN, 100 random samples of CamCAN are used for the reference site and the remaining 341 samples are transformed following Eq.(16) into modified-CamCAN. For the other datasets, the reference site of CamCAN is made of all 441 data samples. Each experiment is repeated randomly 30 times for each criterion and averaged.

Experiments

Five experiments were conducted to gauge the performances of ComBAT when pushed to its limits. In the case of modified-CamCAN, since it contains the same data samples as CamCAN (up to a transformation - Eq.(16)), we report the mean absolute difference (MAD) for both the training and the testing data. As for the other datasets' harmonization, we report the Bhattacharyya goodness-of-fit distance (BD).

Experiment 1: Additive and multiplicative biases

The aim of the first experiment is to illustrate that, as

mentioned in § Mathematical limitations of ComBAT, ComBAT cannot correctly align two populations and properly estimate the variance of the moving site $\hat{\delta}_{iv}^{2*}$ when the two populations have different covariate slopes. As such, these experiments gauge the effect that the bias, slope and variance multiplicative factors have on ComBAT (respectively, A, S and M in Eq. (16)).

Experiment 2: Training sample size The effect of the number of training subjects N from the moving site is evaluated by varying its value from 2 to a maximum number of subjects. In each case, the N samples are randomly selected while maintaining an equal number of males and females. In all cases, we report the training and testing MAD error obtained on the modified-CamCAN dataset.

Experiment 3: Training age range The effect of the training age range is evaluated by varying the range in which the moving site data are sampled. We tested age spans from 10 years to 60 years, and, for each age span, we tested various age groups i.e.:

- 10 years age span : 20 – 30, 30 – 40, ..., 70 – 80
- 20 years age span: 20 – 40, 30 – 50, ..., 70 – 90
- 30 years age span: 20 – 50, 30 – 60, ..., 60 – 90
- ...
- 60 years span: 20 – 80, 30 – 90.
- 70 years span: 20 – 90.

For modified-CamCAN, samples of 32 subjects were used for each age range, which is the maximum number of subjects possible to achieve a male/female balance with CamCAN data. Note that the 80 – 90 age range was not included due to the small number of subjects.

Experiment 4: Sex covariate When harmonizing two populations, two key covariates are typically considered: age and sex. In this experiment, we specifically evaluated the impact of the sex covariate. The objective is twofold: first, to assess how critical the inclusion of this covariate is in the ComBAT harmonization equations, and second, to understand the importance of maintaining a well-balanced representation of males and females in the populations being harmonized.

To achieve this, we harmonized the modified-CamCAN dataset onto the CamCAN dataset under different conditions. These included scenarios with and without the sex covariate incorporated into the ComBAT equations (typically in variables x_{ij} and β_v). Furthermore, we investigated the effect of excluding one of the sexes (i.e., harmonizing populations that are either male-only or balanced). This analysis

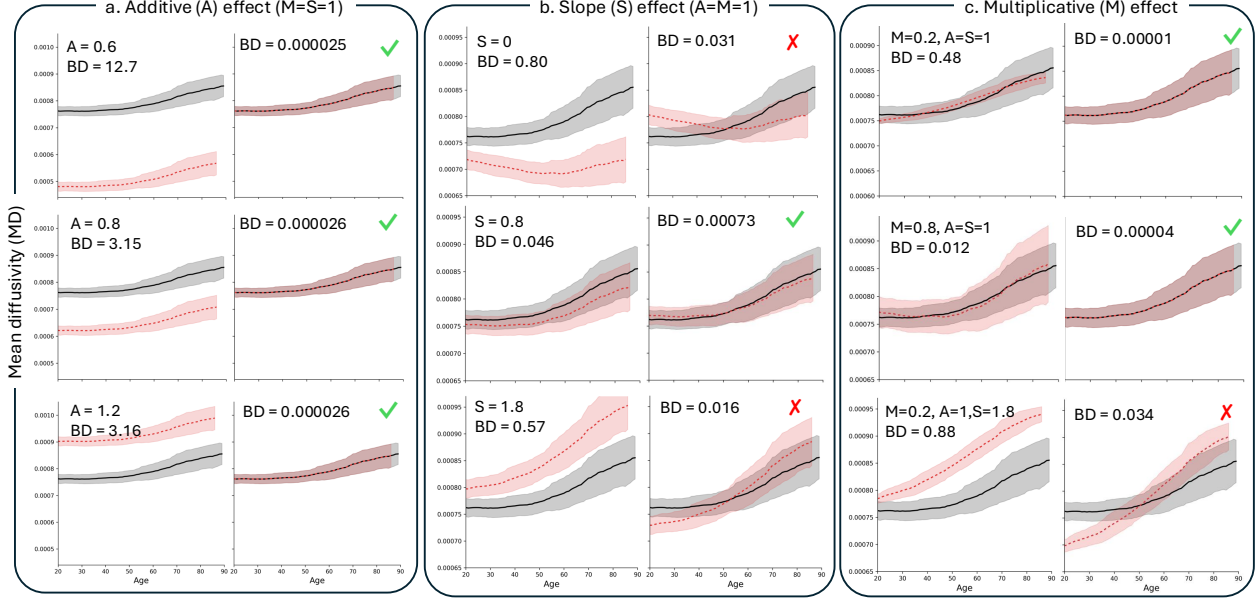


Figure 3: Experiment 1. Harmonization of the Modified-CamCAN population (in gray) on the CamCAN population (in red). Results for different multiplicative factors on (a) the bias (A) (b) the Slope (S) and (c) the noise variance (M) as described in eq. (16). The left columns are the original data and the right columns are the harmonized data. Green checks indicate correct harmonization, red X's indicate poor harmonization.

allows us to measure the influence of both the inclusion of the sex covariate and the population's gender composition on the harmonization performance.

Experiment 5: Pathological populations The effect of pathology was assessed by generating a "control" group and a "pathological" group from the modified CamCAN training sample. The control group includes 100 subjects, which remain constant throughout the experiment. The pathological group also includes 100 subjects and is modified similarly to the first experiment. The additive and multiplicative A and M factors of Eq. (16) vary from 0.8 to 1.20 of the initial value to simulate a more or less different distribution from the control subjects. For this experiment, the age range of the subjects are from 20 and 90 years, with a 50/50 male/female distribution. The effect of pathology is assessed by calculating the harmonizer training and testing error from the healthy control group only (HC-only) as well as for the two healthy control and pathology groups (HC-patho).

Complementary experiments As previously mentioned, for readability, the following results focus on a single metric—mean diffusivity (MD)—and one white matter region—the left arcuate fasciculus (AF left). However, the same experiment was conducted on various other diffusion MRI metrics and white matter regions, all exhibiting trends consistent with those reported in the paper. The supplementary mate-

rial provides results for these additional experiments, including other metrics—fractional anisotropy (FA), isotropic volume fraction (isoVF) from NODDI, and total apparent fiber density (AFDt) from CSD—as well as different brain regions, namely the middle section of the corpus callosum (CC_Mid), the left corticospinal tract (CST_L), and the right inferior fronto-occipital fasciculus (IFOF_R).

Results

Experiment 1: Additive and multiplicative biases

Figure 3 illustrates the effect of the bias, slope, and variance multiplicative factors (A , M , and S) from Eq. (16) on ComBAT harmonization. As shown in column (a), ComBAT effectively compensates for bias effects when $M = S = 1$. Across all cases, the harmonized population exhibits negligible Bhattacharyya distances (BD) on the order of 2.5×10^{-5} . However, as seen on column (b), ComBAT struggles to harmonize data from two sites with significantly different covariate slopes. While harmonization is adequate for a multiplicative slope factor close to 1 like $S = 0.8$, the alignment between the red and black populations deteriorates dramatically for $S = 0$ and $S = 1.8$.

The third column (c) demonstrates that, in the absence of bias and slope factors ($A = S = 1$), ComBAT performs well in compensating for low and high

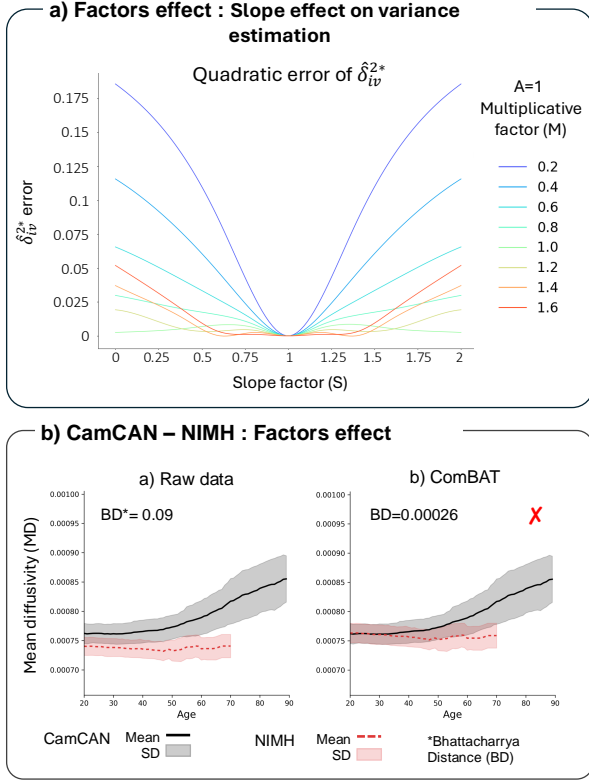


Figure 4: a) The quadratic error in the estimation of the moving site variance δ_{iv}^{2*} for different slope and variance multiplicative factors S and M . b) Harmonization of the mean diffusivity (MD) of the NIMH population (red) onto that of CamCAN (gray). The different slopes between NIMH and CamCAN (left) leads to erroneous harmonization outcomes (right). Red cross indicates poor harmonization.

multiplicative variance factors (i.e., $M = 0.2$ and $M = 1.8$). However, as depicted in the bottom-right figures, when there is a difference in slope between the populations (i.e., $S = 1.8$), ComBAT fails to accurately estimate the population variance δ_{iv}^{2*} .

To illustrate the impact of the slope multiplicative factor S on ComBAT, Figure 4 shows the quadratic error in estimating the moving site variance δ_{iv}^{2*} for varying slope values $S \in [0, 2]$. Each curve represents a unique variance multiplicative factor M . Notably, ComBAT achieves zero error in variance estimation when $S = 1$, i.e. when the covariate slopes are the same for both populations. However, as S deviates from 1 (either decreasing towards 0 or increasing towards 2), the quadratic error in δ_{iv}^{2*} estimation rises.

A similar scenario is illustrated on the bottom of Figure 4, which shows the harmonization of the mean diffusivity (MD) of the NIMH population (red) onto that of CamCAN (gray). The difference in covariate slopes between NIMH and CamCAN (left) leads to erroneous harmonization outcomes (right).

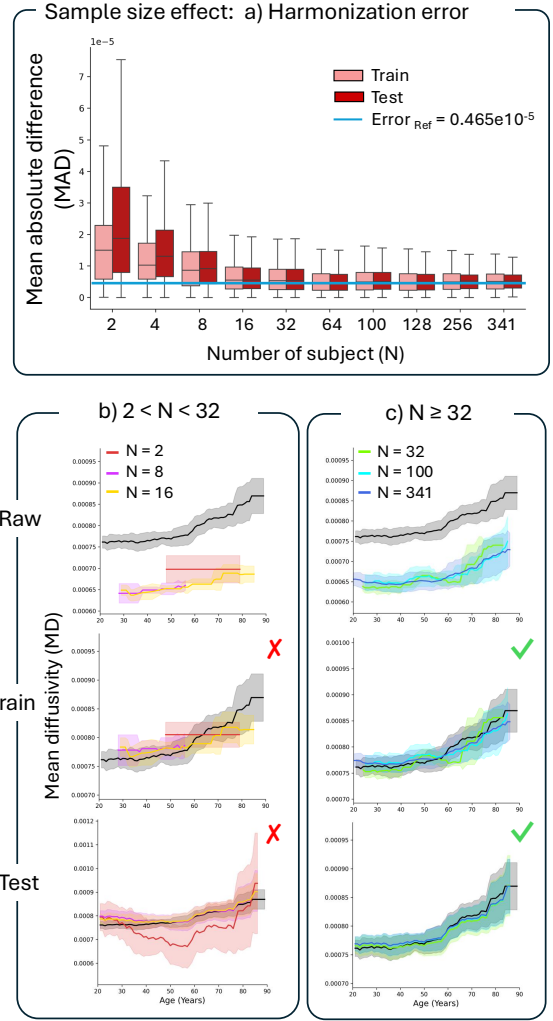


Figure 5: (a) Mean Absolute Difference (MAD) training and testing harmonization errors for various number of training samples N from the Modified-CamCAN moving site. (b) and (c) illustrate the effect of using too few or enough training samples on the training and testing fit. Green checks indicate correct harmonization, red X's indicate poor harmonization.

Experiment 2: Training sample size

The results presented in Figure 5 explore the impact of the number of training subjects N from the moving site on harmonization performance. Figure 5 (a) highlights the relationship between training and testing errors when harmonizing varying numbers of training subjects, ranging from 2 to 341, from the Modified-CamCAN dataset to the reference site. The dashed line in the figure represents the minimum achievable error, which is obtained when the entire dataset is utilized for harmonization.

When examining these results, several patterns become apparent. When a very small number of subjects ($N < 8$) is used, the testing error is significantly higher than the training error. This discrepancy suggests overfitting, as the model struggles to generalize with limited data. As the sample size increases be-

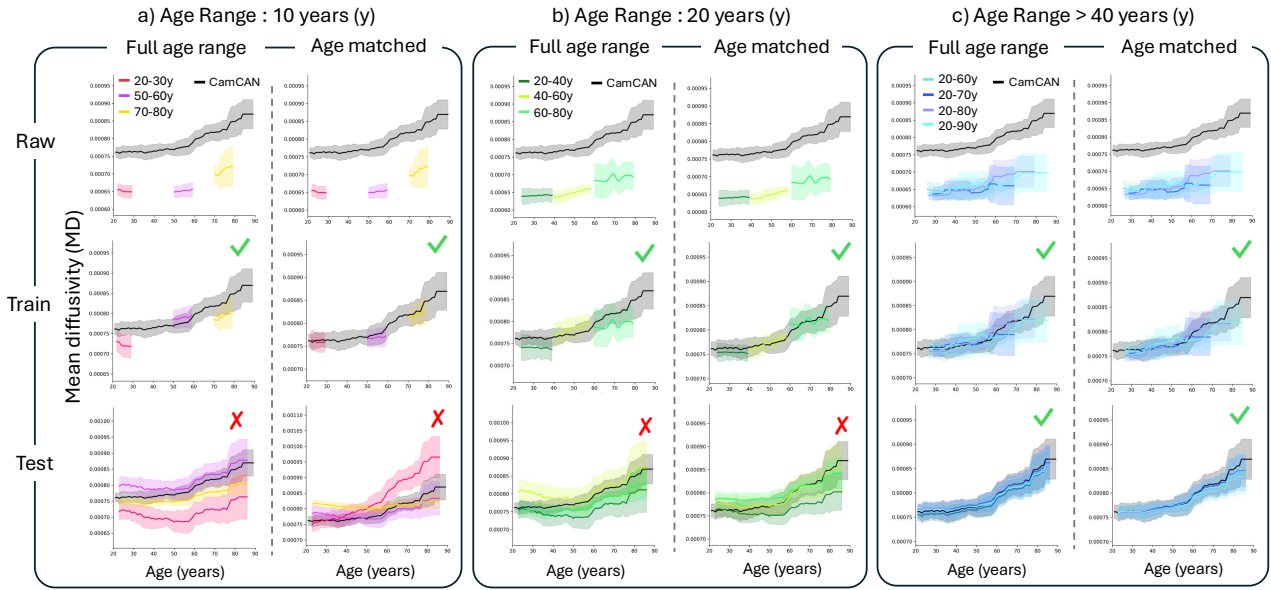


Figure 6: Effect of age range harmonization of the mean diffusivity (MD) metric between the modified CamCAN and CamCAN. Green checks indicate correct harmonization, red X's indicate poor harmonization.

yond $N = 8$ subjects, the testing and training errors begin to decrease, indicating that ComBAT generalizes well even with moderate sample sizes. Importantly, although the training and testing errors approach the minimum achievable error when the sample size reaches 64 subjects or more, it is evident that reasonable harmonization performance can already be achieved with a sample size between 16 and 32 subjects.

This trend is further illustrated in Figures 5 (b) and (c), which provide additional insights into the relationship between sample size and harmonization quality. With 16 or fewer subjects, the testing results remain inconsistent and relatively poor, underscoring the limitations of working with such small datasets. However, as the number of subjects increases to 32 or more, both the training and testing results improve substantially, with harmonization achieving a strong fit to the data.

Experiment 3: Training age range

The harmonization of the Modified-CamCAN moving dataset across different age ranges is depicted in Figure 7 and 6.

Figure 7 reports the training and testing MAD for age ranges from 10 to 70 years. These results emphasize that as the age range widens, the harmonization performance improves, with both training and testing errors stabilizing at a low plateau for age ranges of 40+ years. This suggests that broader age ranges provide more robust estimates of harmonization parameters, improving generalization for unseen data.

More specific harmonization examples for different

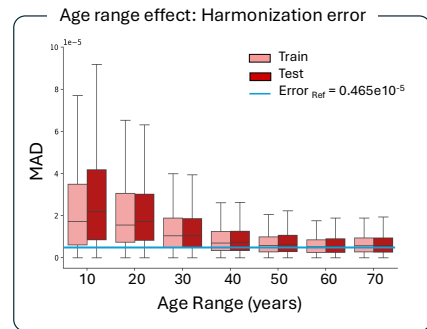


Figure 7: Training and testing mean absolute difference (MAD) harmonization error for age ranges from 10 to 70 years of the Modified-CamCAN dataset.

age ranges are depicted in Figure 6. From left to right, the panels present results for age ranges spanning 10, 20, and 40 years. The first row illustrates unharmonized data for three specific age groups (10 – 20, 50 – 60, and 70 – 80 years in Figure 6(a)), while the second and third rows show the harmonized training and testing data, respectively. In all cases, harmonization outcomes are compared between two approaches: using the full CamCAN age range (20 – 90 years) or restricting to CamCAN subjects whose ages match those of the moving site (i.e., 10 – 20, 50 – 60, and 70 – 80 years for Figure 6(a)).

Across all settings, ComBAT achieves relatively low training errors, particularly when harmonization is performed using reference site subjects whose ages align closely with those in the moving site. This effect is especially pronounced for the 20 – 30 and 70 – 80 year age ranges, where the harmonized train-

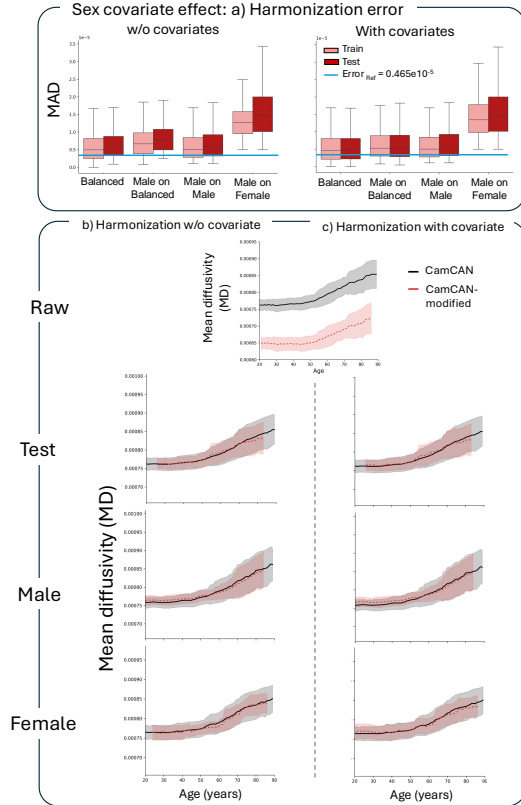


Figure 8: Effect of covariate on Pairwise-ComBAT harmonization of the mean diffusivity (MD) metric between modified CamCAN and CamCAN datasets. *a)* Mean Absolute Difference (MAD) harmonization when considering male-only, female-only and a balance (male+female) populations. *b)* and *c)* harmonization results when using two balanced populations without (*b*) and with (*c*) sex covariate.

ing distribution deviates less from the original black CamCAN distribution. However, examining the testing results reveals a critical limitation: smaller age ranges, such as 10 or 20 years, often result in poor harmonization fits for the testing data. Despite this, the results in Figure 6(c) demonstrate that good training and testing harmonization fits can be achieved when the age range exceeds 40 years.

Experiment 4: Sex covariate

The top panel of Figure 8 illustrates the MAD harmonization error across various scenarios: harmonizing two balanced populations (i.e., equal numbers of males and females), harmonizing a male-only population with a balanced population, harmonizing two male-only populations, and harmonizing a male-only population with a female-only population. Additionally, we assessed the effect of including the sex covariates (x_{ij} and β_v) in the ComBAT equations. The left side of the figure shows results where the sex covariates were excluded from the harmonization equations, while the right side shows results with

these covariates included.

Interestingly, the first three scenarios result in low training and testing harmonization errors, while the fourth—harmonizing a male-only population with a female-only population—exhibits significantly larger errors. While accounting for sex covariates slightly improves the harmonization of a male-only population with a balanced population, this improvement is subtle. These findings emphasize the challenges and limitations of harmonizing highly heterogeneous populations, where covariate adjustments alone may not suffice.

The bottom panel of Figure 8 shows the results of harmonizing two balanced populations with and without incorporating sex covariates in the harmonization equations. The progression begins with the raw data, followed by the harmonized balanced test set, and concludes with visualizations of the harmonized male and female populations. Notably, including the sex covariate in the ComBAT equation does not significantly impact the results when the populations are well-balanced in terms of male and female representation.

Experiment 5: Pathological populations

Figures 9 and 10 present harmonization results when the moving site includes both healthy control (HC) subjects and subjects affected by a pathology. In Figure 9 (a) and (b), the pathological cases (blue dots) are a subset of subjects from the Modified-CamCAN dataset, where a negative bias is introduced in (a) and a positive bias in (b). In both scenarios, the harmonized training and testing data highlight the critical importance of using only HC subjects for harmonization onto a reference, such as CamCAN. Including pathological cases in the harmonization process results in a compressed population, where the harmonized HC and pathological cases are erroneously aligned with the target population (gray).

Additionally, Figure 9 (c) demonstrates that including pathological cases in the training set significantly increases the harmonization error. This issue becomes particularly problematic when the pathology’s bias falls below $A = M = 0.9$ or exceeds $A = M = 1.1$.

Figure 10 illustrates the HC subjects (red-shaded region) and pathological cases (AD and MCI markers) from the 127-GE ADNI site in comparison with the CamCAN dataset. When the harmonization parameters are computed using only HC subjects, the red and gray-shaded populations are perfectly aligned, and the pathological cases remain appropriately distinct as outliers. Conversely, if both HC and pathological cases are used to estimate the ComBAT harmonization parameters, the pathological population

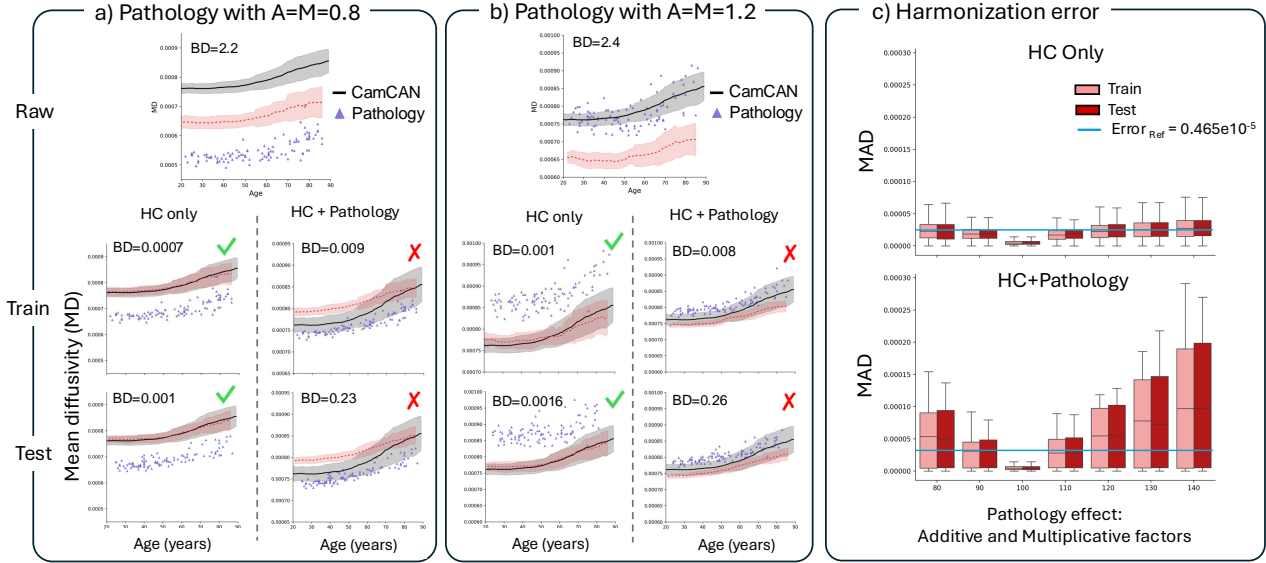


Figure 9: (a) and (b) illustrate a pathological population (purple triangles) exhibiting negative (top left) and positive (middle top) bias relative to a normative population (red). Below these, the harmonization results are shown both with and without the inclusion of pathological cases in the training dataset. Green checks indicate correct harmonization, red X's indicate poor harmonization. (c) presents the harmonization mean absolute difference (MAD) error, comparing scenarios with [bottom] and without [top] the inclusion of pathological cases during training.

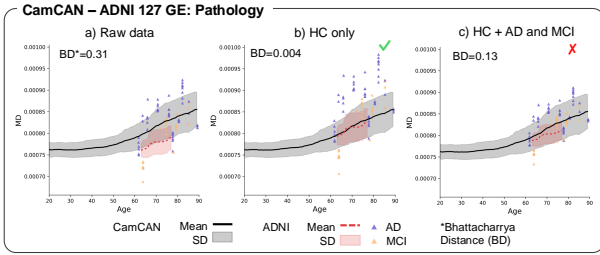


Figure 10: Harmonization of ADNI-127-GE site with CamCAN. a) Raw data, b) Pairwise-ComBAT harmonization from HC group only, c) Pairwise-ComBAT harmonization from HC and pathological group. The gray (target site) and red (moving site) lines show the population mean trend of both sites, and the corresponding light color indicates the standard deviation. Green checks indicate correct harmonization, red X's indicate poor harmonization.

is compressed into the normative range, creating the false impression that these subjects are normal.

Discussion

We evaluated the often-overlooked influence of various factors on the effectiveness of the ComBAT harmonization method, using a pairwise implementation of the technique. Our experiments investigated the effects of site-wise biases, sample size, age range, the sex covariate, and the presence of pathologies. Results demonstrate that ComBAT's performance can be impacted by these factors, which underlines how

ComBAT cannot be used as a black box.

As a general guideline, ComBAT performs well when harmonizing relatively large, well-balanced populations (in terms of age and sex) with substantial inter-population overlap in age distributions and similar age covariate slopes. ComBAT performs also well for compensating additive and multiplicative biases (parameters A and M through our experiments). Our findings also reiterate ComBAT's ability to preserve the biological variability of critical covariates, such as age, while correcting for inter-site differences.

However, ComBAT cannot be used indiscriminately, as it may produce suboptimal harmonization under certain conditions. One prominent issue arises when the age covariate slope differs between the populations being harmonized. In such cases, while the additive bias is compensated, the multiplicative bias is incorrectly estimated, and the slope discrepancy remains uncorrected. As discussed in § Mathematical limitations of ComBAT, this limitation stems from the assumption that the slope β_v is consistent across all sites, which is not always valid [11, 43].

Another challenge occurs when the sample size is too small for the moving site being harmonized to the reference site. Fortin et al. [19], the first to apply ComBAT to dMRI data harmonization, recommended a minimum of $N = 20$ subjects per site for reliable harmonization. Similarly, Orhac et al. [32] reported that ComBAT becomes less reliable for harmonization of PET imaging biomarkers across two sites when sample sizes fall below $N = 30$ subjects

per site. Our results are consistent with these studies, showing that a reasonable harmonization can already be obtained with 16 to 32 subjects and that fewer subjects many result into overfitting (low training error and large testing error).

Another issue emerges when the age range of a population is too narrow (< 20 years). When reference subjects closely match the age range of the moving site (i.e., 10-20 or 70-80), training errors remain relatively low, indicating a good fit to the training data. However, this age-matched approach of adjusting reference distributions based on moving site characteristics does not necessarily result in optimal generalization, as shown by high test errors. This is particularly the case when the age range is restricted to 10 or 20 years, for which test performance deteriorates, leading to inconsistencies in the harmonization, especially for age ranges not included in the training data. In contrast, the improvement in both training and test errors is reached with age ranges of 40 years or greater. This finding is consistent with previous research suggesting that wider age distributions and age range overlap are required for an optimal ComBAT harmonization [29, 26].

Regarding the covariates, Pairwise-ComBAT assumes that all subjects share the same distribution when covariates are not included, i.e. it assumes identical distributions between males and females, which risks suppressing biologically relevant variability by wrongly attributing it to site effects [43, 32]. The inclusion of covariates helps to account for differences in distributions, thereby improving harmonization - especially in cases of demographic imbalance. This is consistent with the findings of Kim et al. [43], who reported that ComBat struggles to harmonize sites with very small and demographically diverse samples unless appropriate covariates are included.

Results also emphasize the importance of handling pathological populations carefully. In clinical studies of brain diseases like Alzheimer's (AD), Multiple Sclerosis (MS) or brain tumours, the site effect is often influenced by differences in clinical status [43, 32, 44]. To prevent site effects from confounding biological variability, previous studies have typically included clinical status as a covariate [43, 44]. In contrast, this study excludes clinical status from the estimation of training parameters, rather than using it as a covariate. When pathological and healthy subjects are mixed, Pairwise-ComBAT tends to compress both pathological and healthy subjects around the target site, thereby reducing population-related variability. The proposed harmonization strategy preserves biological variability while correcting for site effects, thus avoiding bias in the pathological population. Thereby, a recommended strategy is to estimate the

harmonization parameters using only control subjects, temporarily excluding pathological cases. Once estimated, these parameters can then be applied to the pathological subjects. This approach minimizes the risk of confounding disease-related variability with site effects [32].

In conclusion, our findings underscore that the key to successful ComBAT harmonization lies in ensuring that populations are as homogeneous as possible in terms of age range, demographic profiles, sex distribution, covariate slope and health status. Neglecting these considerations may not only lead to poor harmonization during training but also result in catastrophic testing errors.

Recommendations for a good ComBAT harmonization

Given the influence of the factors discussed above, we strongly recommend carefully examining the characteristics of the populations from each site before proceeding with their harmonization. This step ensures that ComBAT's assumptions are met, particularly concerning observed distributions (i.e., additive and multiplicative effects) and sample size, and also helps identify one or more relevant covariates. These covariates can be demographic (i.e., age, sex, or handedness) or clinical (i.e., neurodegenerative disease, treatment, or the presence of a brain abnormality, such as a tumor).

In the light of our experiments, our recommendations are as follows:

- **Data inspection:** ComBAT should never be used as a "magic black box." Always ensure that the populations to be harmonized exhibit distributions that align with ComBAT's assumptions, particularly uniformity across key variables.
- **Covariate slope effect:** The data slope β_v of key co-variables such as age should be approximately the same across all sites. If this condition is not met, the resulting harmonization is likely to be erroneous.
- **Sample size:** At least 16 to 32 subjects should be included when computing the parameters of ComBAT to ensure that the resulting harmonization function generalizes well to all data.
- **Age distributions:** The age range of the moving site's population should span at least 40 years. If this requirement cannot be met, consider using an age-matched ComBAT harmonization, particularly for applications where proper harmonization of the training population is crucial.
- **Sex covariate:** Populations from all sites should have a uniform distribution of male and female subjects. Under no circumstances should a male

predominant population be harmonized with a female predominant population, and vice versa.

- **Disease differences:** For normative modeling applications, always compute the ComBAT harmonization parameters using a group of healthy subjects. These parameters can later on be applied to pathological subjects, reducing the risk of confounding disease-related variability with site effects.

Interestingly, some of our recommendations echos that of Karayumak et al [21] (LinearRISH method) which mention that : "At least 16 to 18 well-matched (sex and age) healthy controls from each site are needed to reliably capture site related differences".

Conclusions and future works

This study rigorously examined the ComBAT harmonization methodology and its variant, Pairwise-ComBAT, in addressing biases across multi-site diffusion MRI datasets. The findings highlight the critical importance of adhering to foundational assumptions, such as demographic consistency, sufficient sample size, and proper covariate representation, to ensure robust harmonization outcomes. While ComBAT demonstrated remarkable efficacy in compensating for additive and multiplicative biases, challenges arise when site-wise demographic distributions or covariate slopes differ significantly. We also provided six recommendations for an optimal application of ComBAT in both research and clinical settings, emphasizing its potential for preserving biological variability and facilitating reproducible science.

Code and Data Availability

The source code and documentation of the Pairwise-ComBAT method as well as the data used in the experimental section will be rendered public upon acceptance of this paper.

Acknowledgments

This work was supported by the ACUITY/CQDM consortium, the Natural Sciences and Engineering Research Council of Canada through its discovery grant program, and the MITACS Acceleration funding program. We are also thankful for the Institutional Université de Sherbrooke Research Chair in Neuroinformatics and NSERC Discovery Grant.

Data collection and sharing for this project was funded by the Alzheimer’s Disease Neuroimaging Initiative (ADNI) (National Institutes of Health Grant U01 AG024904) and DOD ADNI (Department of Defense award number W81XWH-12-2-0012). ADNI

is funded by the National Institute on Aging, the National Institute of Biomedical Imaging and Bio-engineering, and through generous contributions from the following: AbbVie, Alzheimer’s Association; Alzheimer’s Drug Discovery Foundation; Araclon Biotech; BioClinica, Inc.; Biogen; Bristol-Myers Squibb Company; CereSpir, Inc.; Cogstate; Eisai Inc.; Elan Pharmaceuticals, Inc.; Eli Lilly and Company; EuroImmun; F. Hoffmann-La Roche Ltd and its affiliated company Genentech, Inc.; Fujirebio; GE Healthcare; IXICO Ltd.; Janssen Alzheimer Immunotherapy Research & Development, LLC.; Johnson & Johnson Pharmaceutical Research & Development LLC.; Lumosity; Lundbeck; Merck & Co., Inc.; Meso Scale Diagnostics, LLC.; NeuroRx Research; Neurotrack Technologies; Novartis Pharmaceuticals Corporation; Pfizer Inc.; Piramal Imaging; Servier; Takeda Pharmaceutical Company; and Transition Therapeutics. The Canadian Institutes of Health Research is providing funds to support ADNI clinical sites in Canada. Private sector contributions are facilitated by the Foundation for the National Institutes of Health (www.fnih.org). The grantee organization is the Northern California Institute for Research and Education, and the study is coordinated by the Alzheimer’s Therapeutic Research Institute at the University of Southern California. ADNI data are disseminated by the Laboratory for Neuro Imaging at the University of Southern California

References

- [1] Maria A. Di Biase et al. "Mapping human brain charts cross-sectionally and longitudinally". In: *procs of the National Academy of Sciences* 120 (20 May 2023). ISSN: 0027-8424.
- [2] Andre F. Marquand et al. "Understanding Heterogeneity in Clinical Cohorts Using Normative Models: Beyond Case-Control Studies". In: *Biological Psychiatry* 80 (7 Oct. 2016), pp. 552–561. ISSN: 00063223.
- [3] Saige Rutherford et al. "Evidence for embracing normative modeling". In: *eLife* 12 (Mar. 2023). ISSN: 2050-084X.
- [4] Serena Verdi et al. "Beyond the average patient: how neuroimaging models can address heterogeneity in dementia". In: *Brain* 144 (10 Nov. 2021), pp. 2946–2953. ISSN: 0006-8950.
- [5] Julio E. Villalón-Reina et al. "Multi-site Normative Modeling of Diffusion Tensor Imaging Metrics Using Hierarchical Bayesian Regression". In: *proc of MICCAI*. 2022, pp. 207–217.
- [6] Suheyra Cetin-Karayumak et al. "Harmonized diffusion MRI data and white matter measures from the Adolescent Brain Cognitive Development Study". In: *Scientific Data* 11 (1 Feb. 2024), p. 249. ISSN: 2052-4463.
- [7] Fengling Hu et al. "Image harmonization: A review of statistical and deep learning methods for removing batch effects and evaluation metrics for effective harmonization". In: *NeuroImage* 274 (2023), p. 120125.
- [8] Khoi Minh Huynh et al. "Multi-Site Harmonization of Diffusion MRI Data via Method of Moments". In: *IEEE Trans. on Med. Ima.* 38 (7 July 2019), pp. 1599–1609. ISSN: 0278-0062.

- [9] Daniel Moyer et al. "Scanner invariant representations for diffusion MRI harmonization". In: *Magnetic Resonance in Medicine* 84 (4 Oct. 2020), pp. 2174–2189. ISSN: 0740-3194.
- [10] Kurt G. Schilling et al. "Fiber tractography bundle segmentation depends on scanner effects, vendor effects, acquisition resolution, diffusion sampling scheme, diffusion sensitization, and bundle segmentation workflow". In: *NeuroImage* 242 (Nov. 2021), p. 118451. ISSN: 10538119.
- [11] Johanna MM Bayer et al. "Site effects how-to and when: An overview of retrospective techniques to accommodate site effects in multi-site neuroimaging analyses". In: *Frontiers in neurology* 13 (2022), p. 923988.
- [12] Karl G Helmer et al. "Multi-site study of diffusion metric variability: effects of site, vendor, field strength, and echo time on regions-of-interest and histogram-bin analyses". In: *Medical Imaging 2016: Biomedical Applications in Molecular, Structural, and Functional Imaging*. Vol. 9788. SPIE. 2016, pp. 729–738.
- [13] Maíra Siqueira Pinto et al. "Harmonization of Brain Diffusion MRI: Concepts and Methods". In: *Frontiers in Neuroscience* 14 (May 2020). ISSN: 1662-453X.
- [14] Andrew A Chen et al. "Mitigating site effects in covariance for machine learning in neuroimaging data". In: *Human brain mapping* 43.4 (2022), pp. 1179–1195.
- [15] Alberto De Luca et al. "Cross-site harmonization of multi-shell diffusion MRI measures based on rotational invariant spherical harmonics (RISH)". In: *NeuroImage* 259 (Oct. 2022), p. 119439. ISSN: 10538119.
- [16] Hannah Horng et al. "Generalized ComBat harmonization methods for radiomic features with multi-modal distributions and multiple batch effects". In: *Scientific Reports* 12 (1 Mar. 2022), p. 4493. ISSN: 2045-2322.
- [17] Fengling Hu et al. "DeepComBat: A Statistically Motivated, Hyperparameter-Robust, Deep Learning Approach to Harmonization of Neuroimaging Data". In: *bioRxiv* (Apr. 2023), p. 2023.04.24.537396.
- [18] W. Evan Johnson, Cheng Li, and Ariel Rabinovic. "Adjusting batch effects in microarray expression data using empirical Bayes methods". In: *Biostatistics* 8 (1 Jan. 2007), pp. 118–127. ISSN: 1468-4357.
- [19] Jean-Philippe Fortin et al. "Harmonization of multi-site diffusion tensor imaging data". In: *NeuroImage* 161 (Nov. 2017), pp. 149–170. ISSN: 10538119.
- [20] Chantal MW Tax et al. "Cross-scanner and cross-protocol diffusion MRI data harmonisation: A benchmark database and evaluation of algorithms". In: *NeuroImage* 195 (2019), pp. 285–299.
- [21] Suheyla Cetin Karayumak et al. "Retrospective harmonization of multi-site diffusion MRI data acquired with different acquisition parameters". In: *NeuroImage* 184 (Jan. 2019), pp. 180–200. ISSN: 10538119.
- [22] Jean-Philippe Fortin et al. "Harmonization of cortical thickness measurements across scanners and sites". In: *NeuroImage* 167 (Feb. 2018), pp. 104–120. ISSN: 10538119.
- [23] Joaquim Radua and et al. "Increased power by harmonizing structural MRI site differences with the ComBat batch adjustment method in ENIGMA". In: *NeuroImage* 218 (Sept. 2020), p. 116956. ISSN: 10538119.
- [24] Leon Y Cai et al. "MASiVar: Multisite, multiscanner, and multisubject acquisitions for studying variability in diffusion weighted MRI". In: *Magnetic resonance in medicine* 86.6 (2021), pp. 3304–3320.
- [25] Doris Leithner et al. "Impact of ComBat harmonization on PET radiomics-based tissue classification: a dual-center PET/MRI and PET/CT study". In: *Journal of Nuclear Medicine* 63.10 (2022), pp. 1611–1616.
- [26] Joanne C. Beer et al. "Longitudinal ComBat: A method for harmonizing longitudinal multi-scanner imaging data". In: *NeuroImage* 220 (Oct. 2020), p. 117129. ISSN: 10538119.
- [27] Alexandre Carré et al. "AutoComBat: a generic method for harmonizing MRI-based radiomic features". In: *Scientific Reports* 12.1 (2022), p. 12762.
- [28] R. Da-ano et al. "Performance comparison of modified ComBat for harmonization of radiomic features for multicenter studies". In: *Scientific Reports* 10 (1 June 2020), p. 10248. ISSN: 2045-2322.
- [29] Raymond Pomponio et al. "Harmonization of large MRI datasets for the analysis of brain imaging patterns throughout the lifespan". In: *NeuroImage* 208 (Mar. 2020), p. 116450. ISSN: 10538119.
- [30] Bao Hoang et al. "Distributed Harmonization: Federated Clustered Batch Effect Adjustment and Generalization". In: *in proc of SIGKDD*. 2024, pp. 5105–5115.
- [31] Chiara Marzi et al. "Efficacy of MRI data harmonization in the age of machine learning: a multicenter study across 36 datasets." In: *Sci Data* 115.11 (2024).
- [32] Fanny Orhlac et al. "A guide to ComBat harmonization of imaging biomarkers in multicenter studies". In: *Journal of Nuclear Medicine* 63.2 (2022), pp. 172–179.
- [33] Pravesh Parekh et al. "Sample size requirement for achieving multisite harmonization using structural brain MRI features". In: *NeuroImage* 264 (2022), p. 119768.
- [34] Meredith A Shafto et al. "The Cambridge Centre for Ageing and Neuroscience (Cam-CAN) study protocol: a cross-sectional, lifespan, multidisciplinary examination of healthy cognitive ageing". In: *BMC Neurology* 14 (1 Dec. 2014), p. 204. ISSN: 1471-2377.
- [35] Jason R. Taylor et al. "The Cambridge Centre for Ageing and Neuroscience (Cam-CAN) data repository: Structural and functional MRI, MEG, and cognitive data from a cross-sectional adult lifespan sample". In: *NeuroImage* 144 (Jan. 2017), pp. 262–269. ISSN: 10538119.
- [36] Paul S. Aisen et al. "Clinical core of the Alzheimer's disease neuroimaging initiative: Progress and plans". In: *Alzheimer's & Dementia* 6 (3 May 2010), pp. 239–246. ISSN: 1552-5260.
- [37] Randy L. Gollub et al. "The MCIC Collection: A Shared Repository of Multi-Modal, Multi-Site Brain Image Data from a Clinical Investigation of Schizophrenia". In: *Neuroinformatics* 11 (3 July 2013), pp. 367–388.
- [38] Seyed Mostafa Kia et al. "Closing the life-cycle of normative modeling using federated hierarchical Bayesian regression". In: *PLoS One* 17.12 (Dec. 2022).
- [39] Allison C Nugent et al. "The NIMH Healthy Research Volunteer Dataset". 2024.
- [40] Guillaume Theaud et al. "TractoFlow: A robust, efficient and reproducible diffusion MRI pipeline leveraging Nextflow & Singularity". In: *NeuroImage* 218 (Sept. 2020), p. 116889. ISSN: 1053-8119.
- [41] Maxime Descoteaux et al. "Deterministic and probabilistic tractography based on complex fibre orientation distributions". In: *IEEE trans. on med. ima.* 28.2 (2008), pp. 269–286.
- [42] Xiaoxiao Qi and Konstantinos Arfanakis. "Regionconnect: Rapidly extracting standardized brain connectivity information in voxel-wise neuroimaging studies". In: *Neuroimage* 225 (2021), p. 117462.

- [43] Michael E Kim et al. "Empirical assessment of the assumptions of ComBat with diffusion tensor imaging". In: *Jour of Med Ima* 11.2 (2024), pp. 024011–024011.
- [44] Russell T Shinohara et al. "Volumetric analysis from a harmonized multisite brain MRI study of a single subject with multiple sclerosis". In: *American Journal of Neuroradiology* 38.8 (2017), pp. 1501–1509.

Supplementary material

This document contains complementary results to those presented in the paper.

Figures 11 to 16 complement Figure 3 in the paper. Figures 11 to 13 illustrate the effect of variations in the slope of the covariate on three metrics—fractional anisotropy (FA), isotropic volume fraction (isoVF), and apparent fiber density (AFD)—measured in the left arcuate fasciculus (AFL). Figures 14 to 16 depict the same experiment but for mean diffusivity (MD), as in Figure 3, measured in the middle corpus callosum (CC_Mid), the left corticospinal tract (CST_L), and the right inferior fronto-occipital fasciculus (IFOF_R).

Figures 17 and 18 relate to Figures 5b and 5c in the paper. Figure 17 shows the effect of using a small number of samples (fewer than 32) versus a larger number of samples (32 and above) on the AFD, FA, and isoVF metrics measured in the AFL white matter region. Figure 18 presents similar results for the AFD metric measured in the CST_L, CC_Mid, and IFOF_R white matter regions.

Figures 19 to 24 correspond to Figure 6 in the paper. Figures 19 to 21 illustrate the effect of using small age ranges on the AFD, FA, and isoVF metrics measured in the AFL white matter region. Figures 22 to 24 show similar results for the AFD metric measured in the CC_Mid, CST_L, and IFOF_R white matter regions.

Figures 25 to 30 correspond to Figure 9 in the paper. Figures 25 to 27 demonstrate the effect of adding pathological data to the harmonization pool when analyzing the AFD, FA, and isoVF metrics in the AFL white matter region. Figures 28 to 30 present similar results for the AFD metric measured in the CC_Mid, CST_L, and IFOF_R white matter regions.

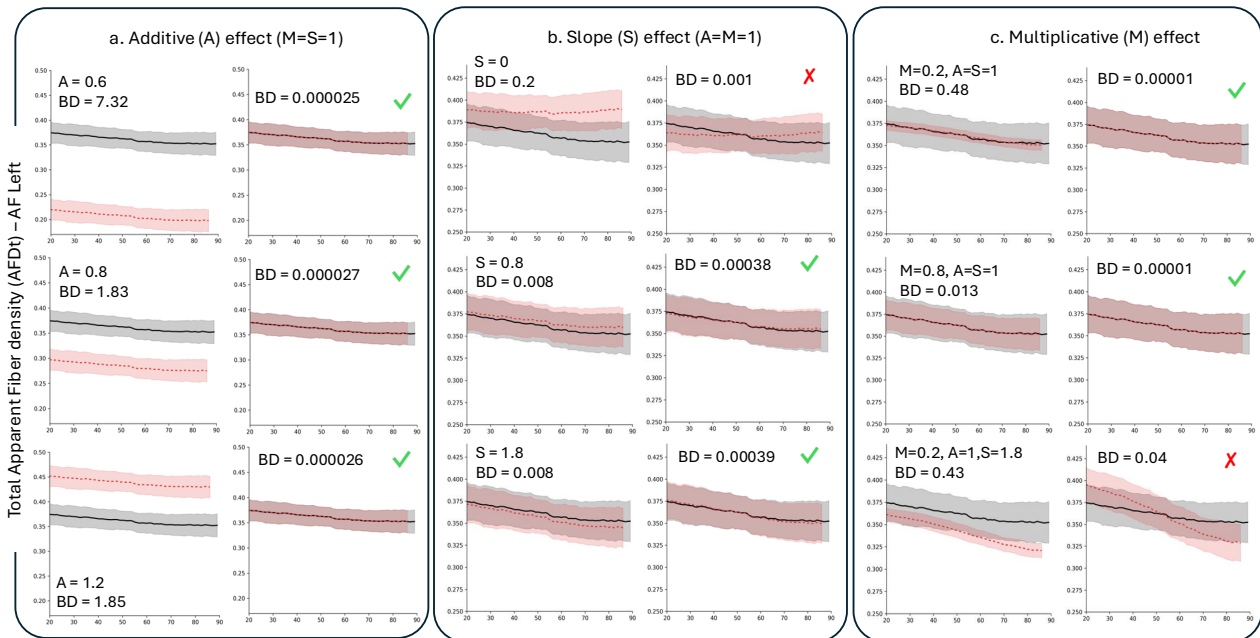


Figure 11: This illustration is complementary to figure 3 in the paper.

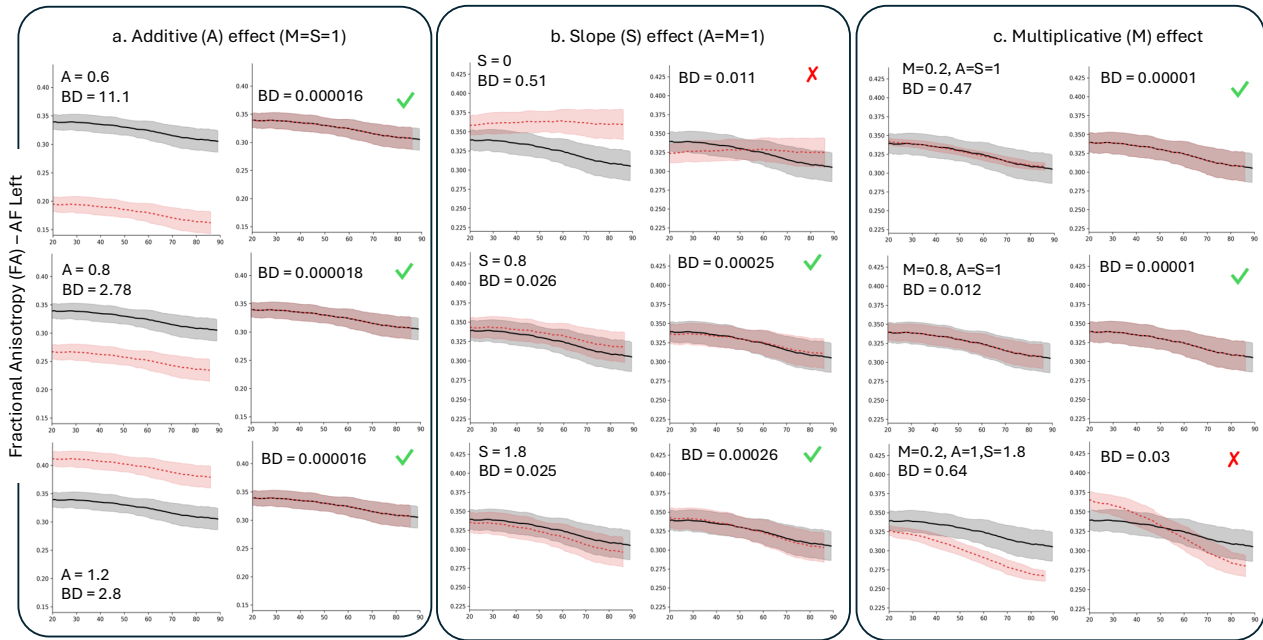


Figure 12: This illustration is complementary to figure 3 in the paper.

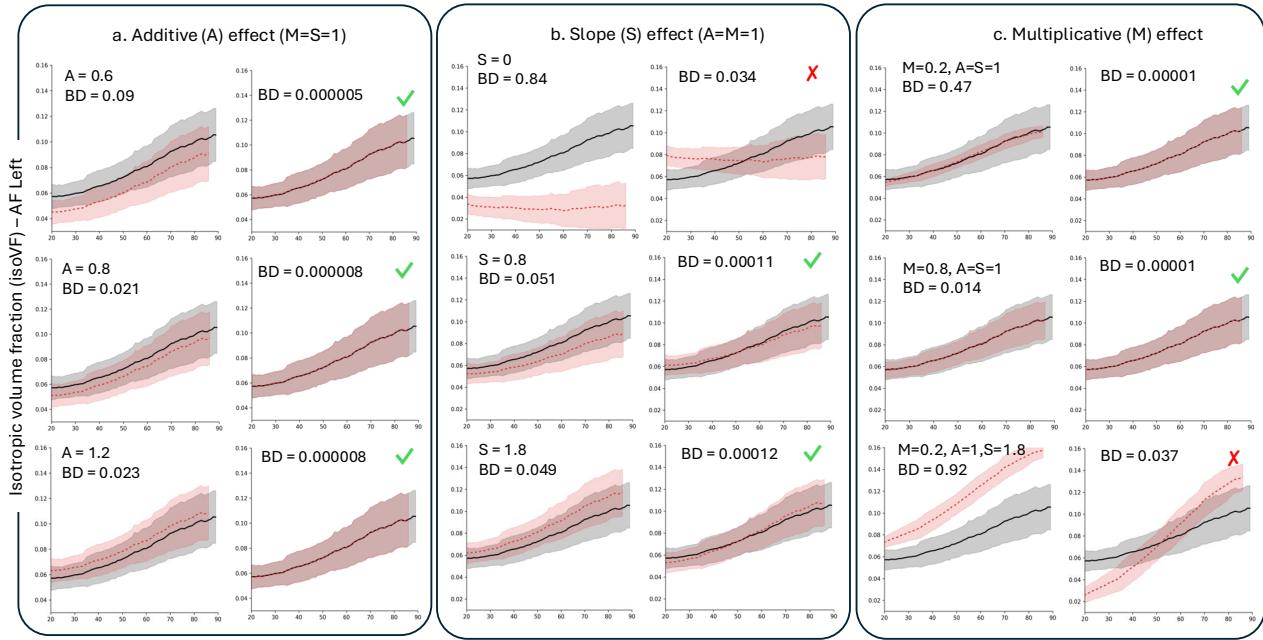


Figure 13: This illustration is complementary to figure 3 in the paper.

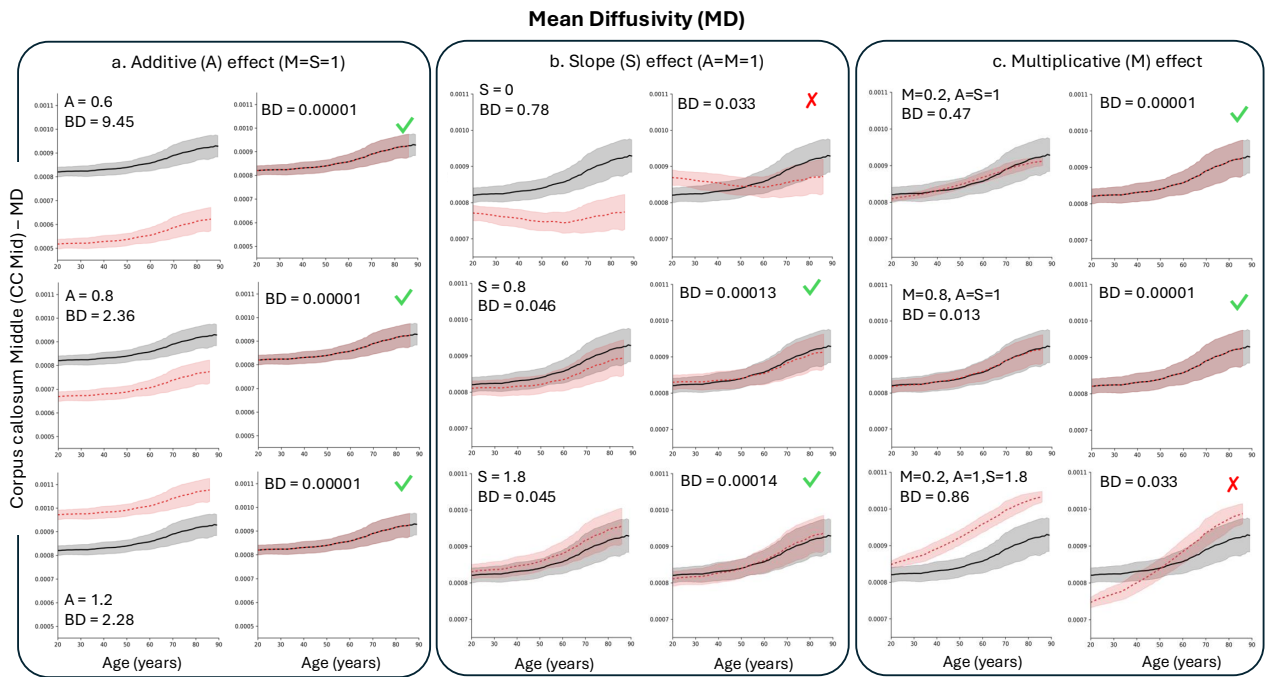


Figure 14: This illustration is complementary to figure 3 in the paper.

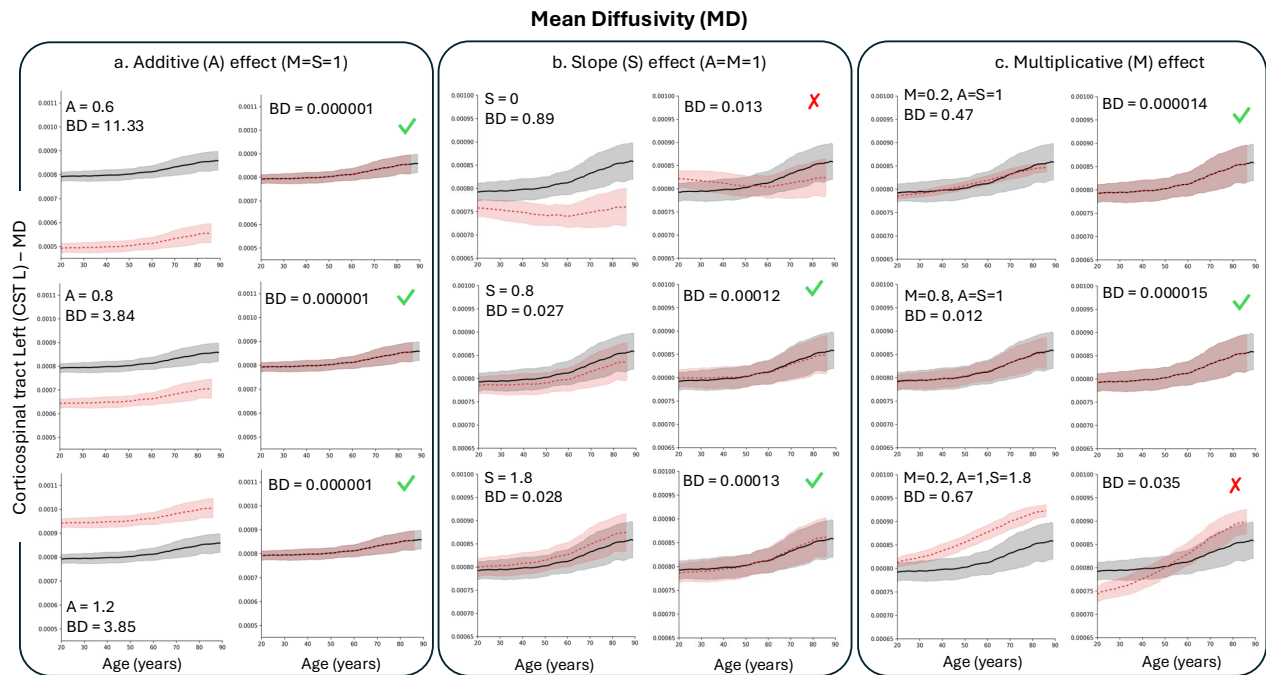


Figure 15: This illustration is complementary to figure 3 in the paper.

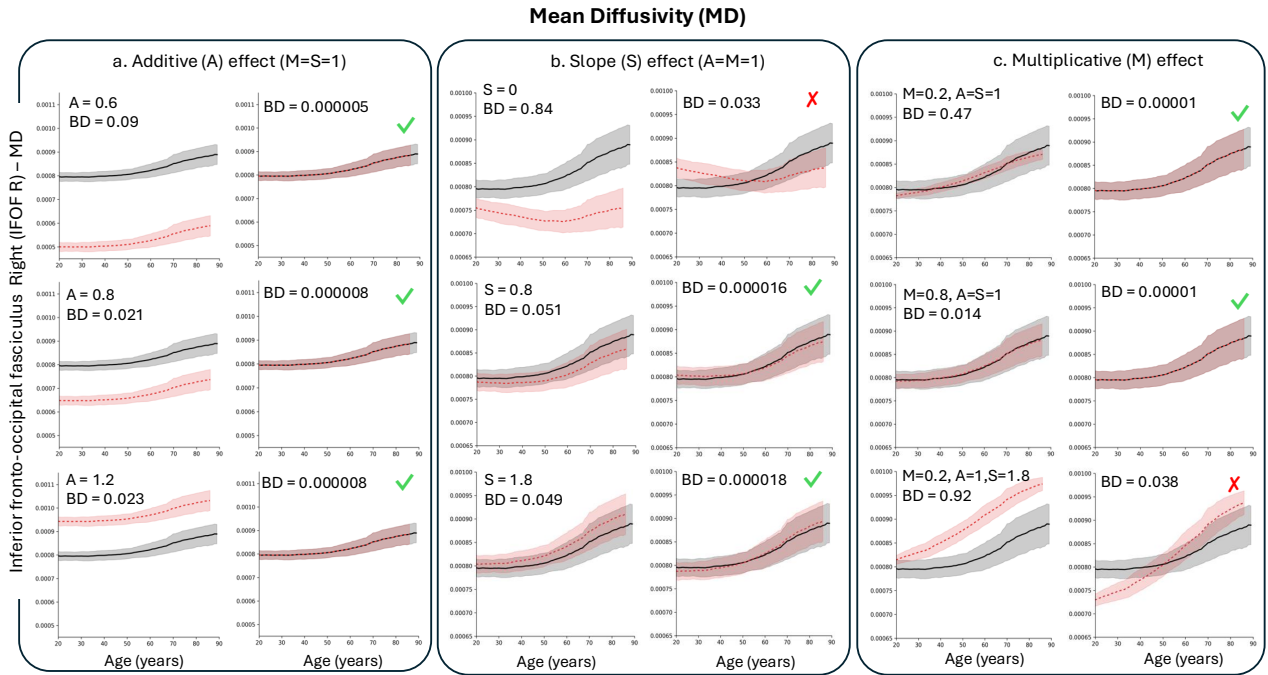


Figure 16: This illustration is complementary to figure 3 in the paper.

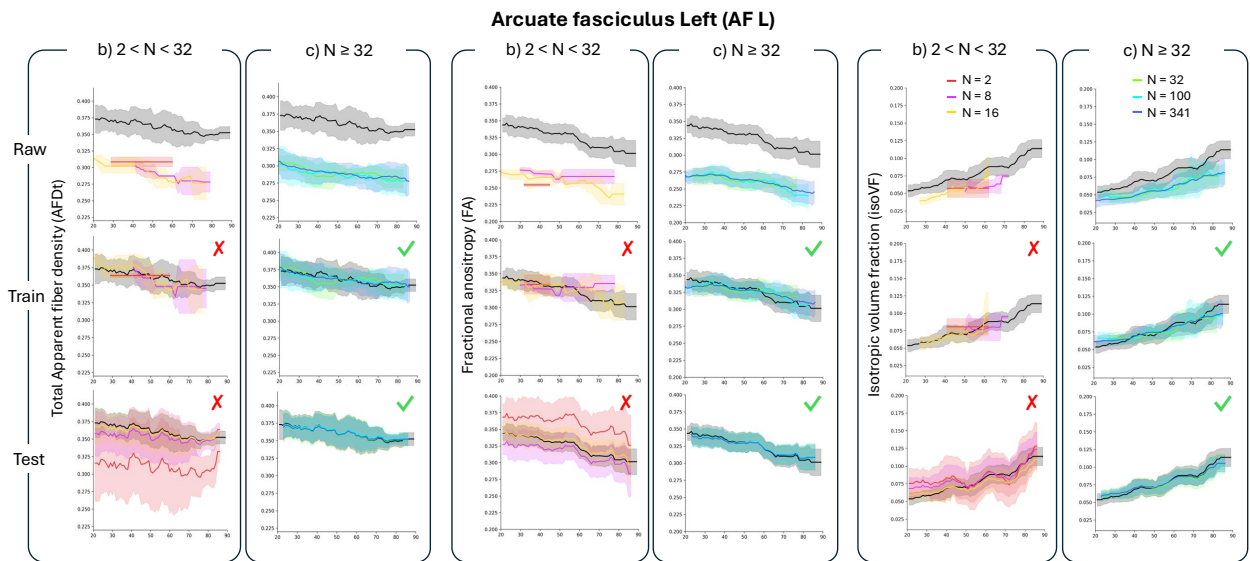


Figure 17: This illustration is complementary to figure 5 in the paper.

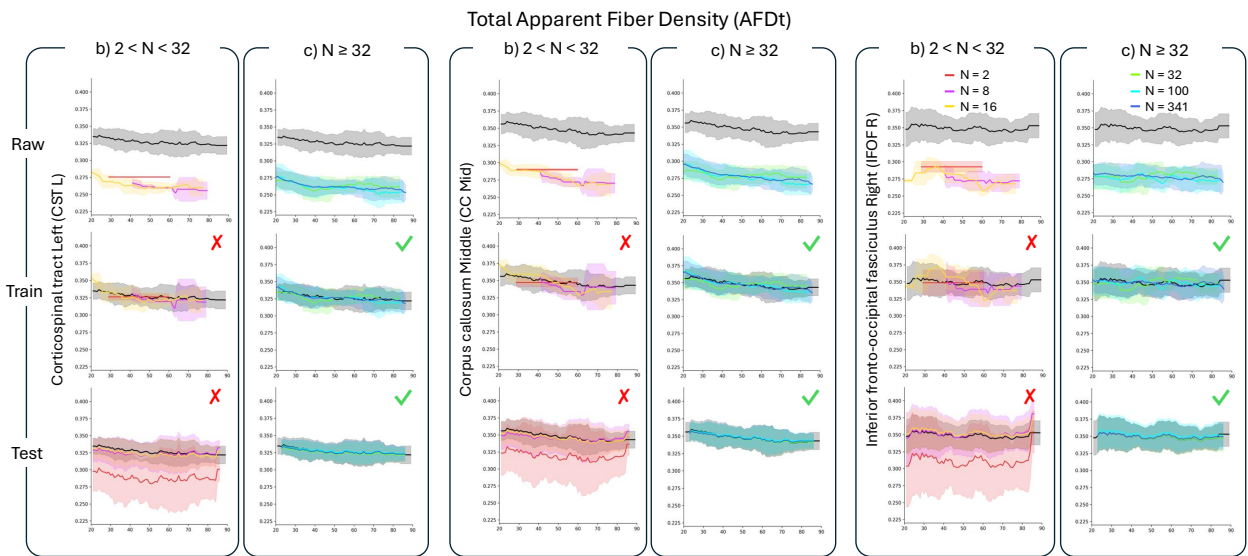


Figure 18: This illustration is complementary to figure 5 in the paper.

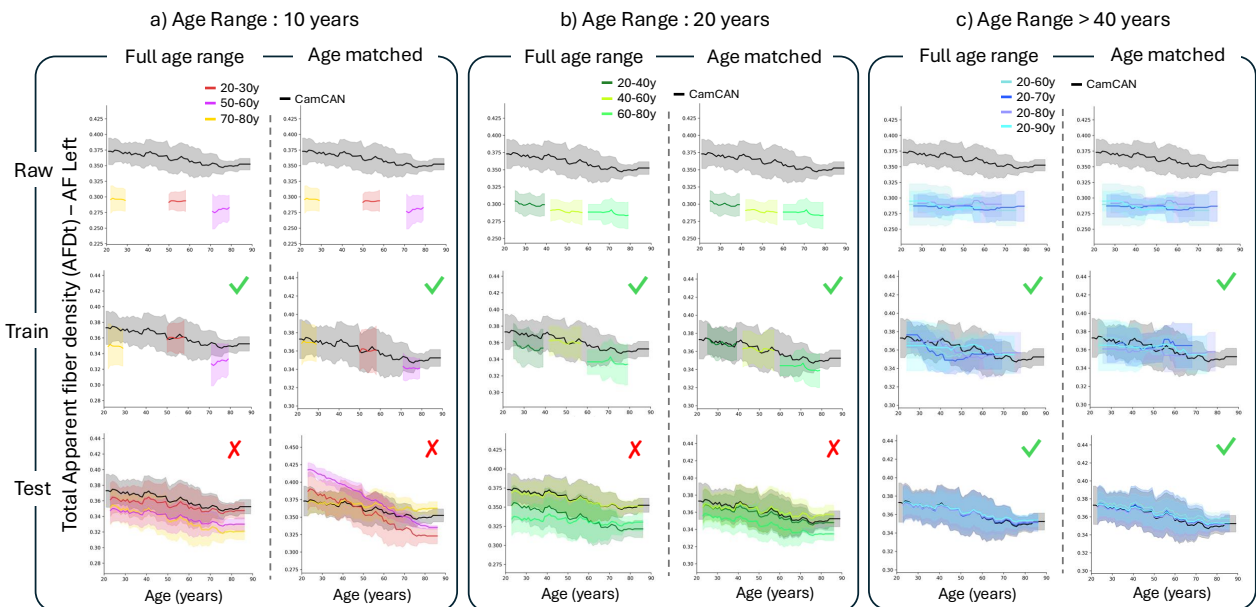


Figure 19: This illustration is complementary to figure 6 in the paper.

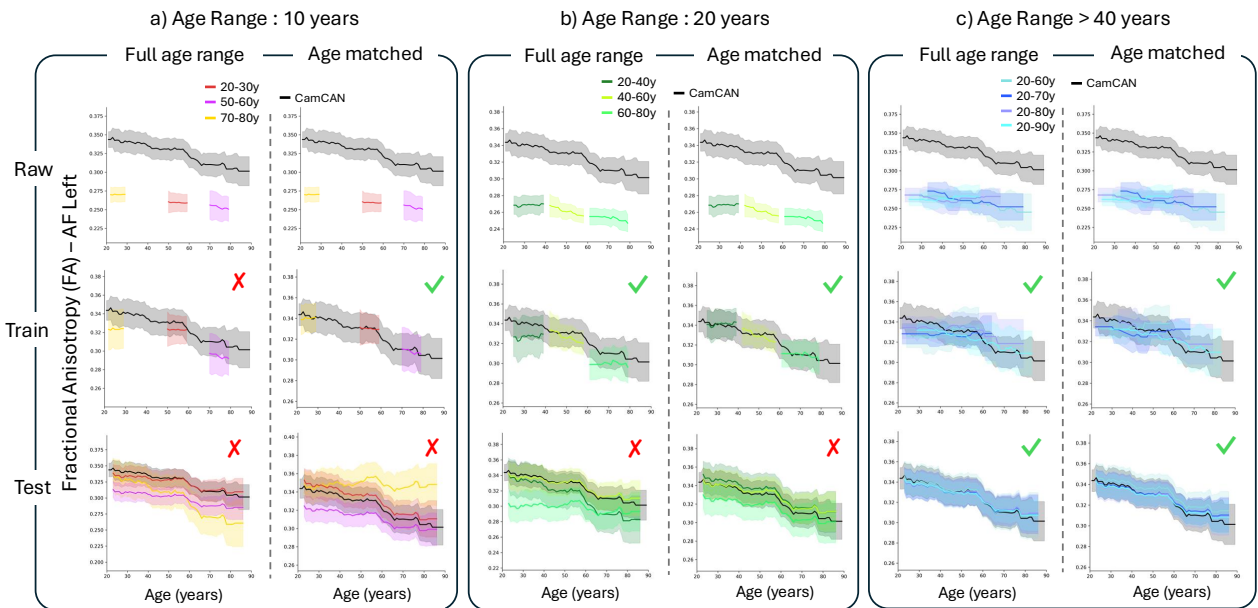


Figure 20: This illustration is complementary to figure 6 in the paper.

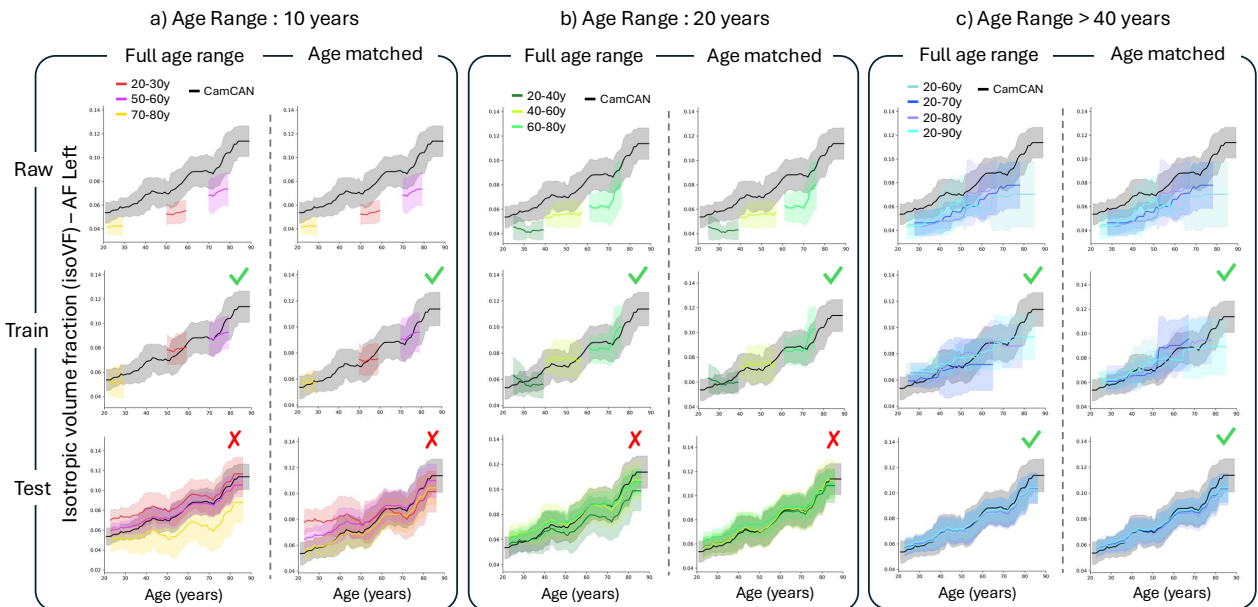


Figure 21: This illustration is complementary to figure 6 in the paper.

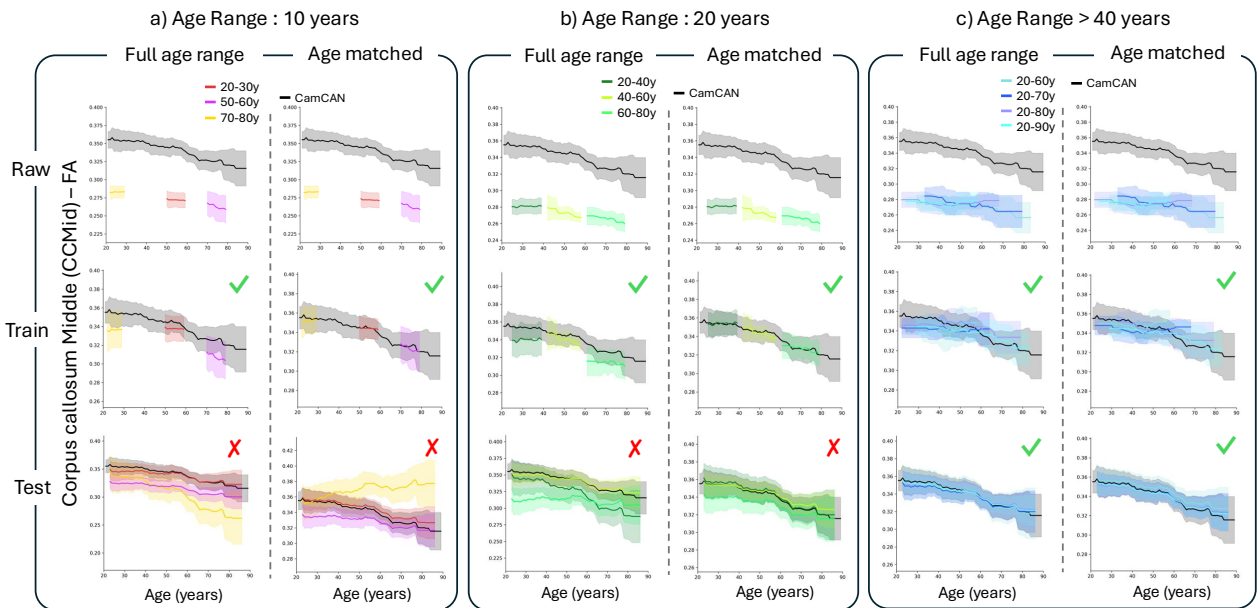


Figure 22: This illustration is complementary to figure 6 in the paper.

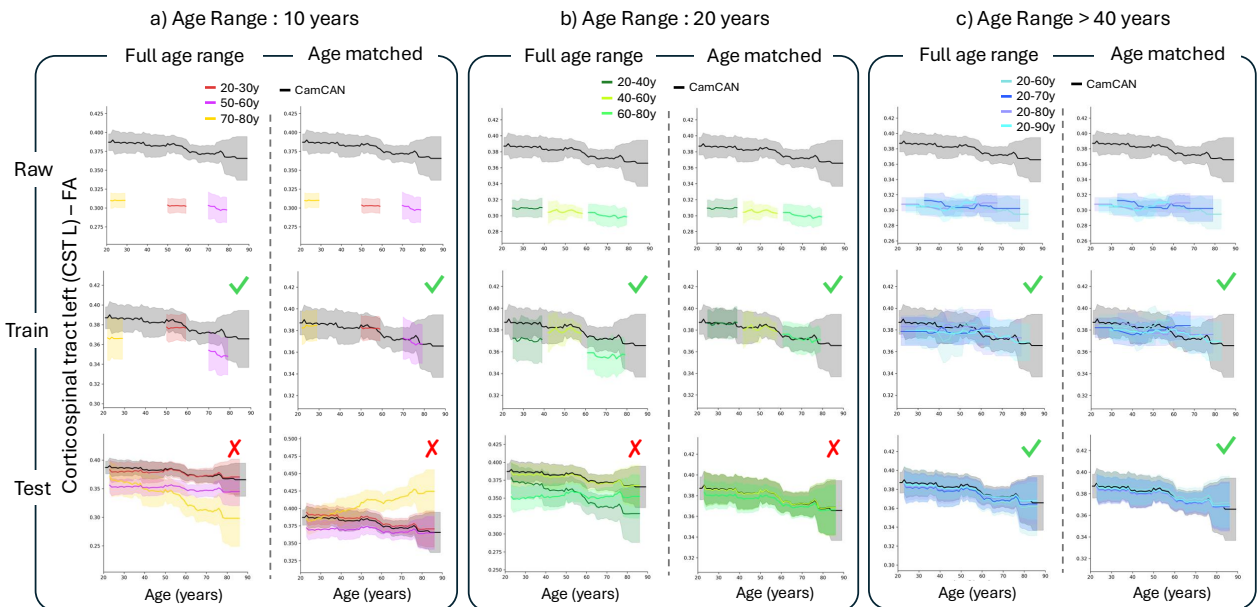


Figure 23: This illustration is complementary to figure 6 in the paper.

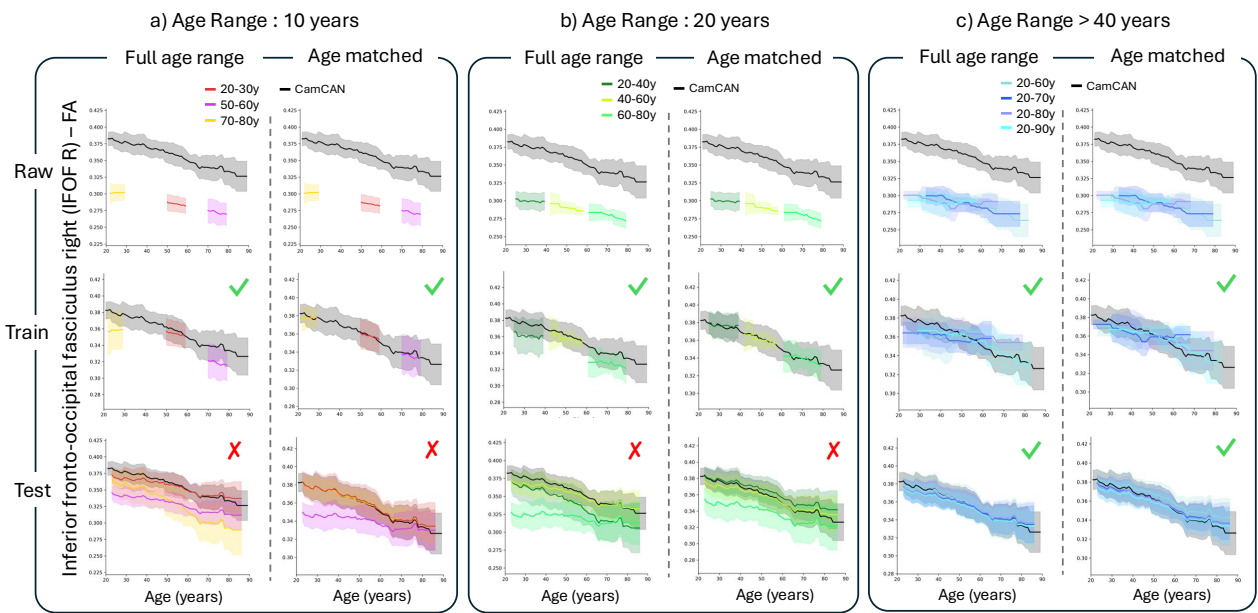


Figure 24: This illustration is complementary to figure 6 in the paper.

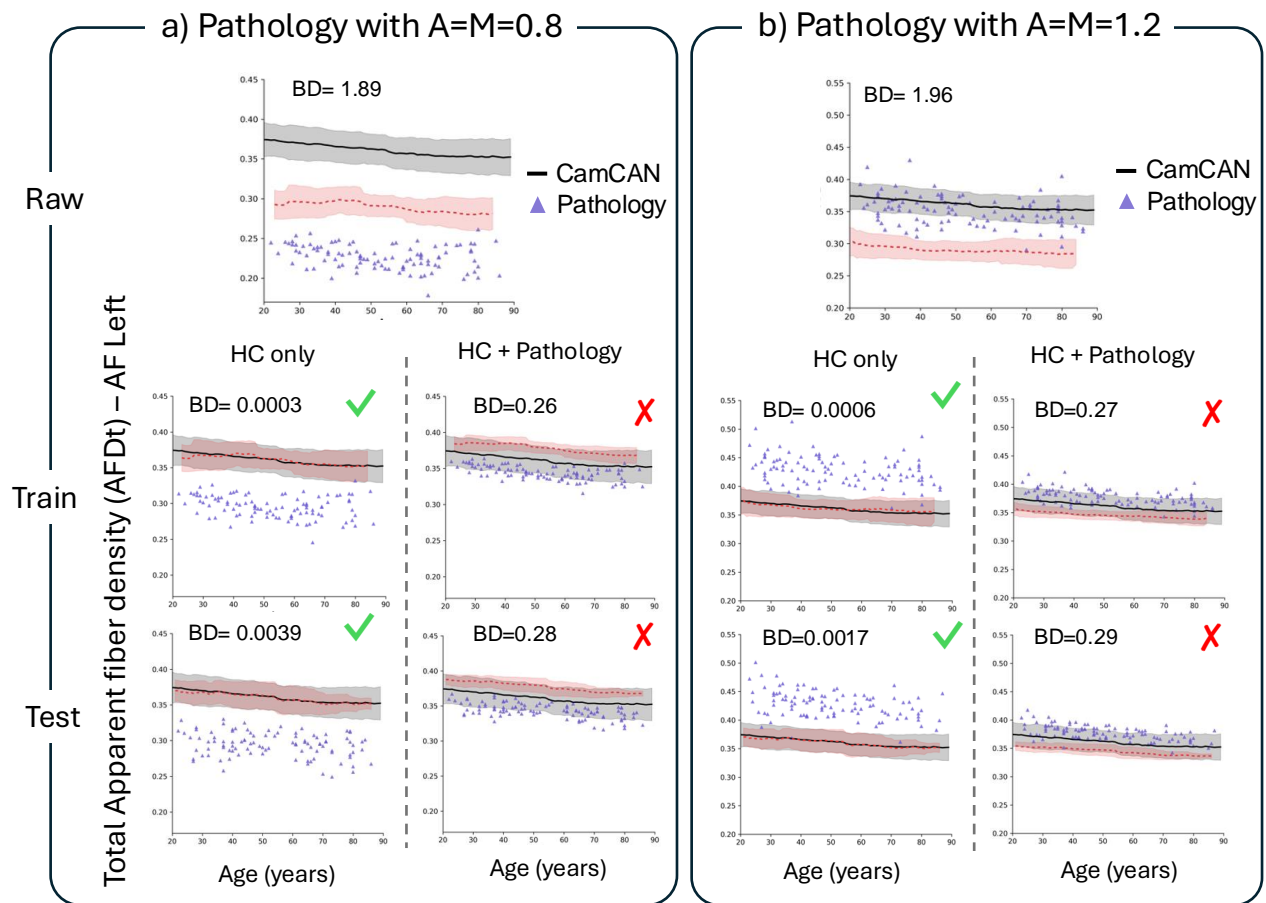


Figure 25: This illustration is complementary to figure 9 in the paper.

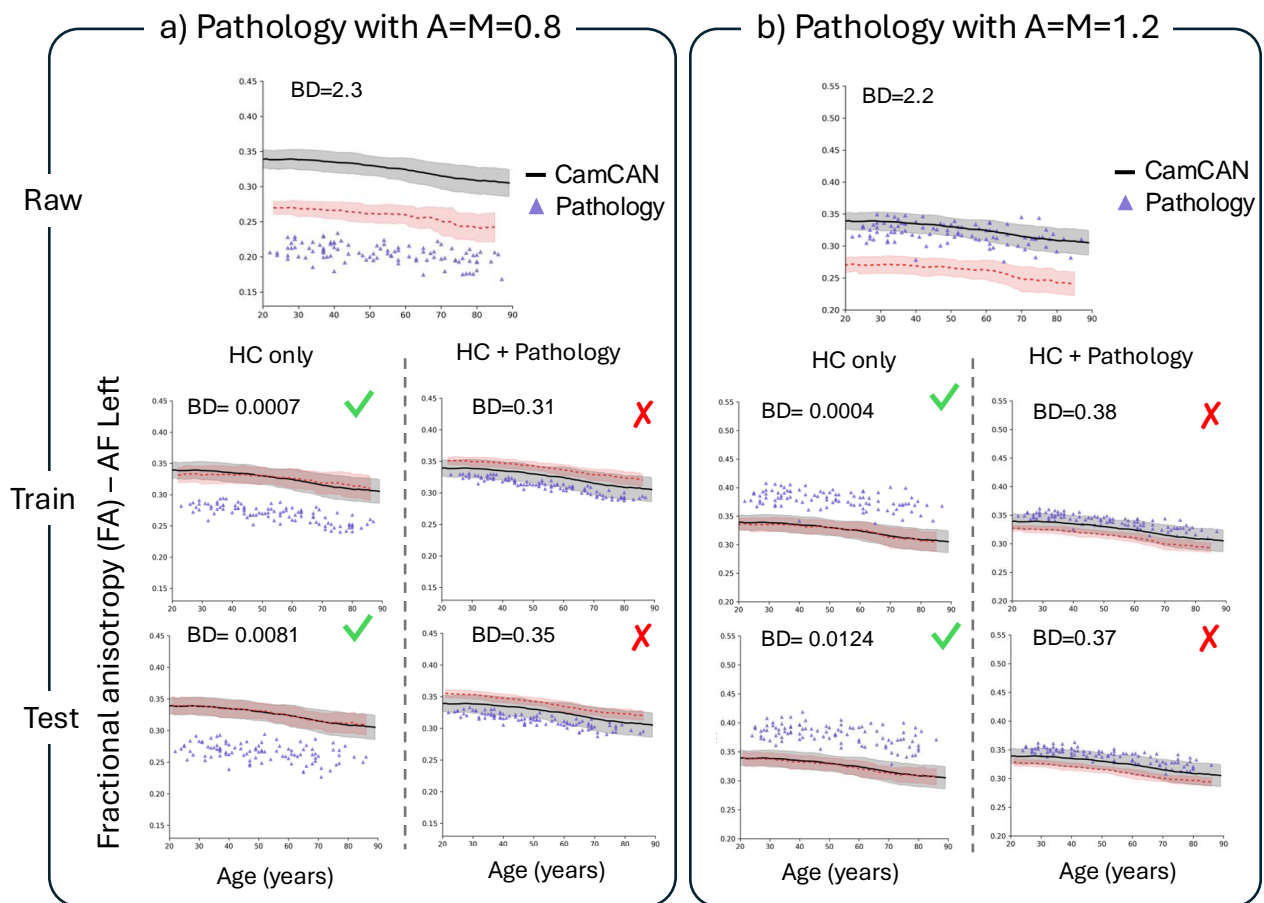


Figure 26: This illustration is complementary to figure 9 in the paper.

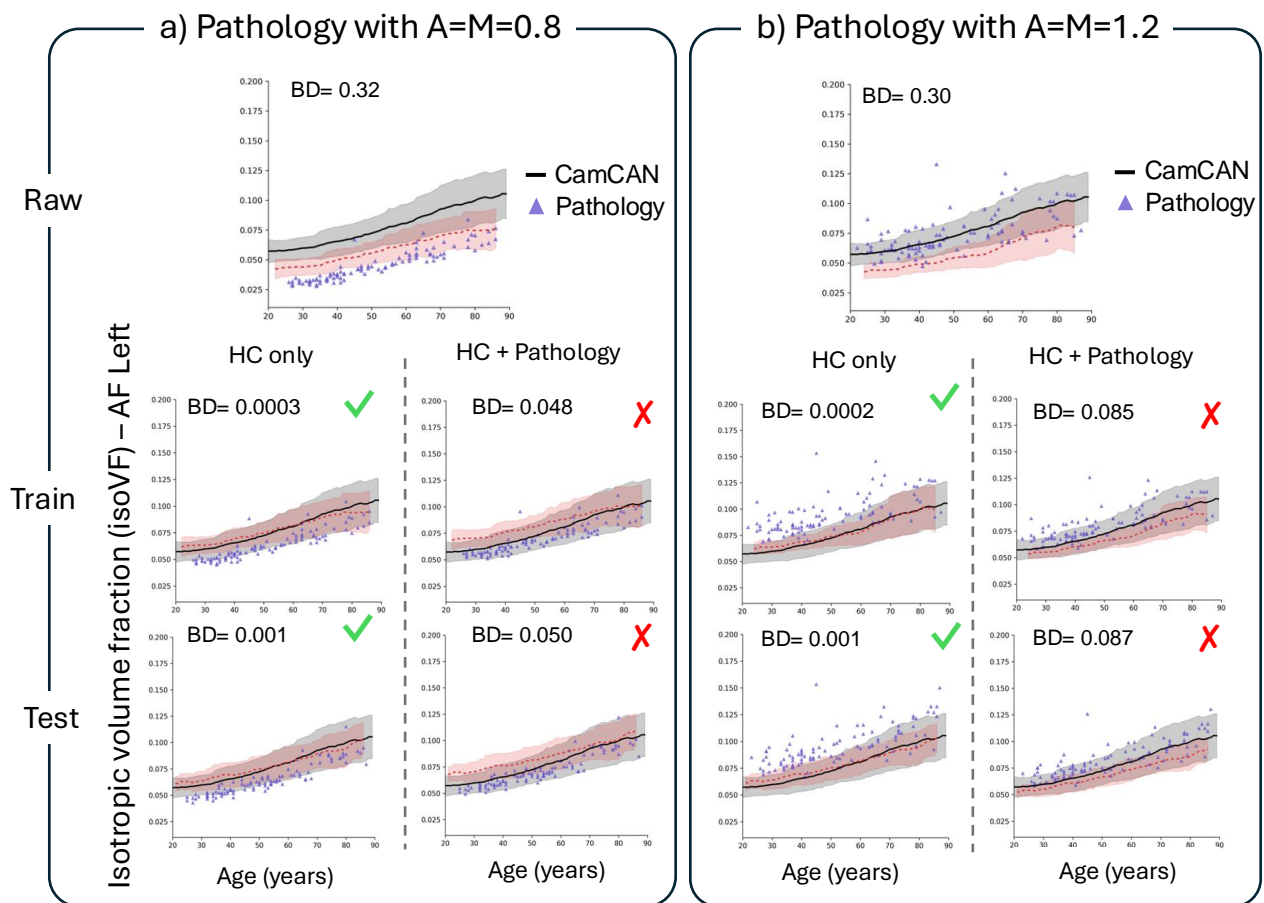


Figure 27: This illustration is complementary to figure 9 in the paper.

Corpus callosum Middle (CC Mid)

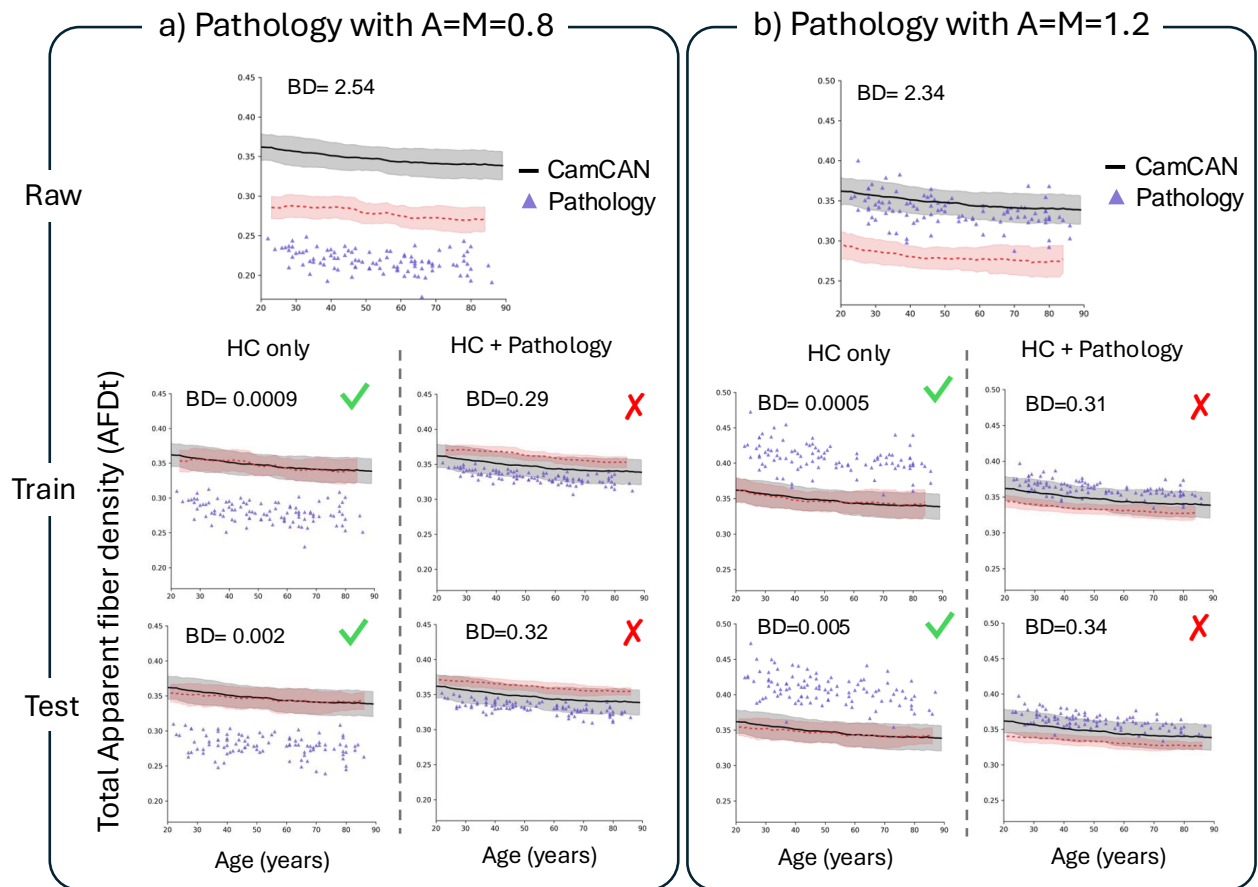


Figure 28: This illustration is complementary to figure 9 in the paper.

Corticospinal tract Left (CST L)

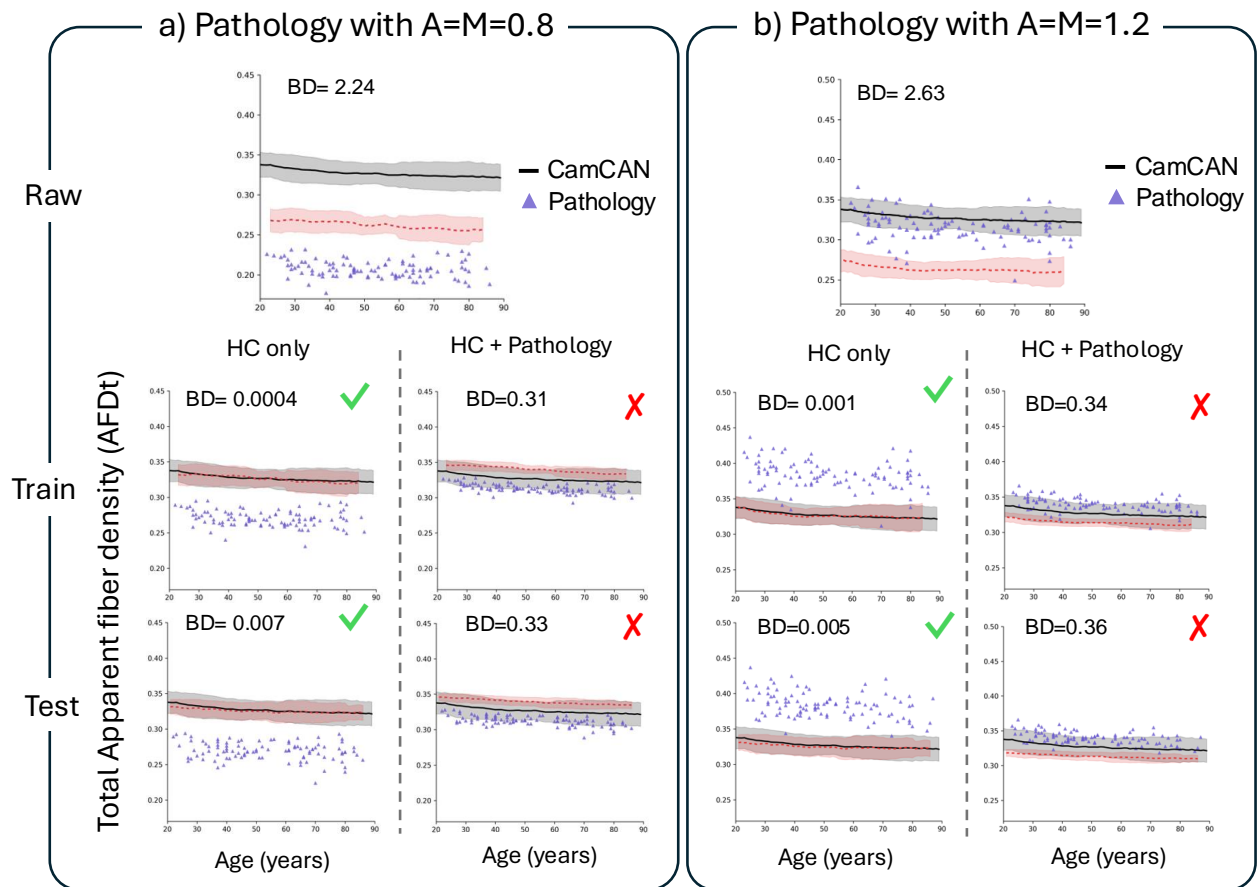


Figure 29: This illustration is complementary to figure 9 in the paper.

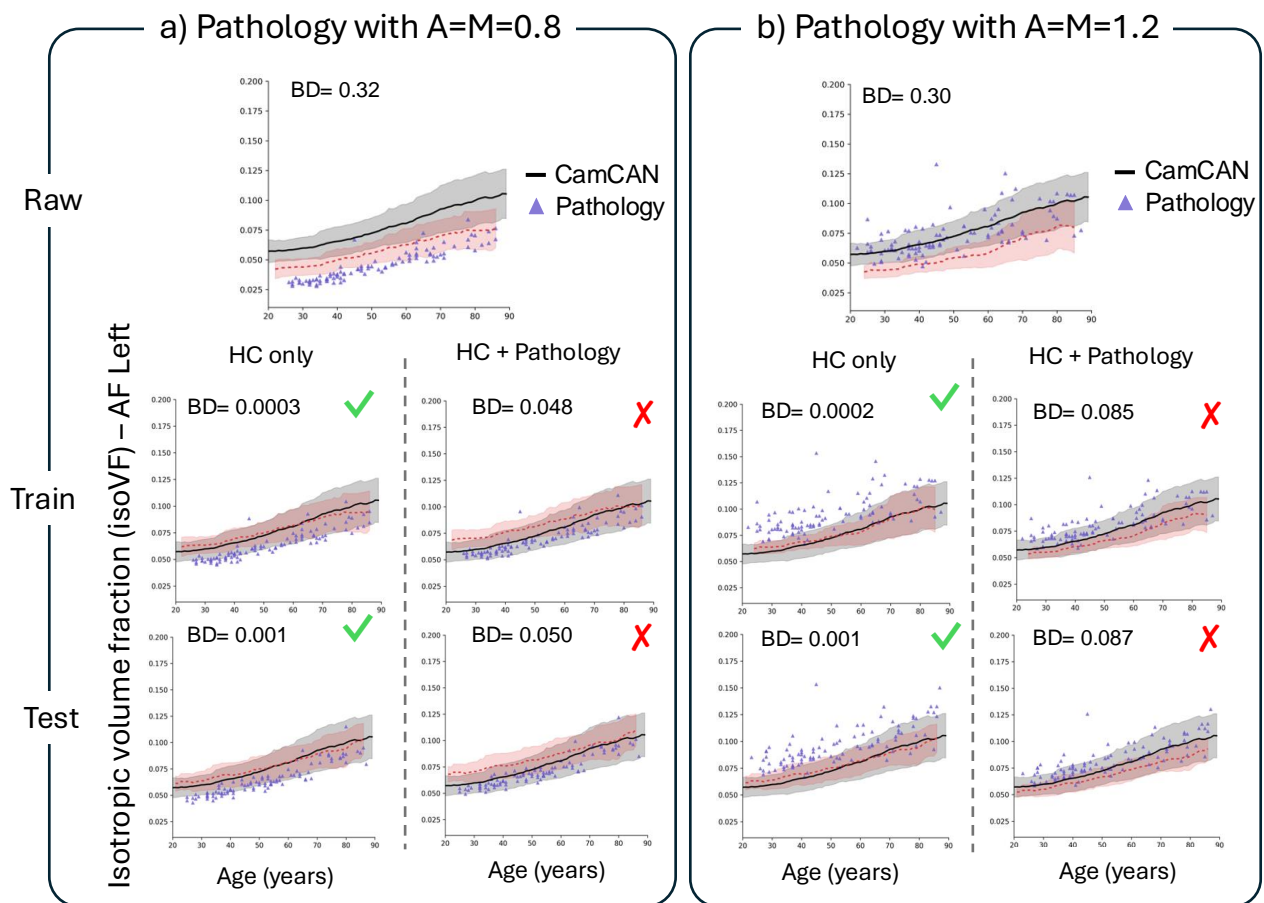


Figure 30: This illustration is complementary to figure 9 in the paper.